LUNDS
UNIVERSITET

Formability Evaluation
Development of an objective method for determining the formability of sheet metal during pressing operations

Charles Ower

May 2023

Supervisor: Volodymyr Bushlya

CODEN:LUTMDN/(TMMV-5351)/1-87/2023

Faculty of Production and Materials Engineering
Lund University

Abstract

This project investigates the possibility of using material thickness measurements of pressed stainless steel (316L) and titanium (grade 1) sheet metal to evaluate material formability. The ultimate goal of this project is to replace the current subjective visual material formability evaluation with an objective method. This project attempts to build relationships between material surface defects that are visually identified and the material thickness which is measured using 3D laser scanning. Formability evaluation methods are compared to asses the strength of these relationships and the feasibility of replacing the current evaluation method.

Acknowledgements

My thanks, first and foremost, go to the help and support given by Jens Rassmus, Mathias Agmell, Volodymyr Bushlya and Daniel Klint. I would also like to thank the host company, Alfa Laval and Lund University for the opportunities afforded to me during this Masters Thesis Project.

Contents

Nomenclature List

Abbreviations

FLD	Forming Limit Diagram
FLC	Forming Limit Curve
FEM	Finite Element Method
Ti	Titanium
316L	Stainless Steel (grade 316, low carbon)
EL	Material elongation at failure

Symbols

α	Principal Stress Ratio
β	Principal Strain Ratio
σ	True Stress
ϵ	True Strain
t	thickness

1 Introduction

Alfa Laval is one of the largest producers of heat exchangers. Pressing sheet metal into complex and accurate parts is one of the core operations in the manufacturing of heat exchanges, Figure 1.1. Therefore it is very important that the forming characteristics and behaviour of the sheet metal blanks is well understood and supply is regularly evaluated. A reduction in the formability of the supply can result in cracks and other surface defects during forming operations, which leads to production downtime, reduction in quality and increased waste. Formability evaluation is used to identify the forming characteristic of supply and is used to reject supply that does not meet production standards.

Figure 1.1: Partial Assemble Large Heat Exchanger, Showing Pressed Heat Exchanger Plate

At Alfa Laval, the current formability evaluation method relies on a visual inspection of a test pressing performed by a trained technician to identify defects, such as necking and cracks at defined areas on the surface of the pressing. The following issues have been

identified with the current formability evaluation method;

- Surface defect classification can be subjective
- Some surface defects are difficult to identify with the unaided eye, due to their size and the reflectivity of the material
- Evaluation technicians require special and regular training

As surface defects, such as necking, is a result of unstable material thinning in a local area, it is proposed that surface defects can be identified through the analysis of the material thickness. 3D scanning of the test pressings is the proposed method for measuring the material thickness.

1.1 Research Questions

The objective of this thesis was to answer the following question:

1. Can material thickness measurements be used to evaluate sheet metal material formability and replace the current visual formality evaluation?

1.2 Objectives

This project has 4 objectives:

- Objective 1: To verify that 3D scanning can be used to measure material thickness and other typical pressing defects
- Objective 2: To identify relationship between material thickness and surface defects
- Objective 3: To evaluate material formability based on the material thickness and compare predictions to results from the current formability evaluation
- Objective 4: To provide physical explanations of the identified relationships

1.3 Structure of Thesis

This thesis is structured as follows:

Chapter 2: Background and Context Definition and background on forming and formability.

Chapter 3: Method Outline of the pressing procedure, current visual evaluation method and the procedure for scanning the test plates and obtaining the material thickness

Chapter 4: Results Current visual evaluation formability results, material thickness results obtained from 3D scans of test plates and an estimate of the strain conditions in the pressed plates

Chapter 5: Discussion Identification and testing of relationships between material thickness and formability score, as well as physical interpretation of results including effects of strain conditions

Chapter 6: Conclusion Answering of the research question, evaluation of project objectives and proposed future work

2 Background and Context

2.1 What is Forming?

Sheet metal forming is an important manufacturing method that allows for the production of complex and intricate shapes. Forming can be achieved in a number of different ways, such as blanking and piercing, bending, section bending, stretching, hole extrusion, stamping or draw die forming, tube forming, fluid forming, coining, ironing and deep drawing (Z. Marciniak et. al [1]). In reality, most industrial forming process involve a combination of the above mentioned processes.

Stamping or draw die forming is widely used in the automotive and heat exchanger industries as it is able to produce complex shapes with high speed and accuracy (A. Awasthi et. al [2]). Parts are formed by forcing blanks over a punch in a draw die and, depending on how the blank is held, material is drawn or stretched to varying degrees, Figure 2.1. The success and reliability of the stamping process is greatly dependent on the design of the punch and die tool, the material properties of the blank and the tribological conditions on the contact surface of the part and tool [1]. It is not only important that the final part had the correct dimensions, but it is vital that part thinning is not to severe and the part is free from defects such as localized necking or cracks.

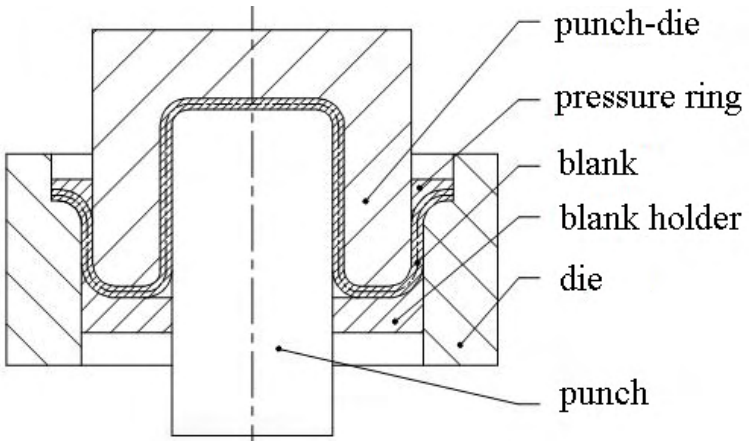

Figure 2.1: Schematic of Sheet Metal Forming in a Press [3]

2.2 What is Formability?

There is no strict definition of formability, however metallic material formability is often described as the ability of a material to plastically deform without damaging [1]. Different parameters can be used to quantify formability depending on intended forming operation Parameters include; fracture strain, forming limits, deep drawability and ductility. In sheet metal forming operations, forming limits are often used to asses and compare the formability of different metals and alloys [4].

2.2.1 Factors that Influence Formability

Material formability is dependent on the material micro structure, which includes; grain size, grain boundary, material state, composition and work hardening. Formability is also dependent on outside factors such as; temperature, load conditions and strain rates.

2.2.2 Formability Parameters

A materials ability to be plastically deformed under uniaxial tension (Figure 2.2) is usually illustrated using the engineering stress strain curve (Figure 2.3). The shape of this curve between the material's yield and ultimate stress as well as the ratio between these two stresses provides insight into the material's ductility and strain hardening rate, which are good indicators of formability [5]. Uniaxial tensile tests are widely used in the classification of material properties as these tests are well understood, standardized, easy to perform and generally are independent of test cross section area and length [1]. It is standard practice for a manufacture to perform uniaxial tensile tests on each material heat, and therefore the yield and ultimate stress for a material heat are readily available.

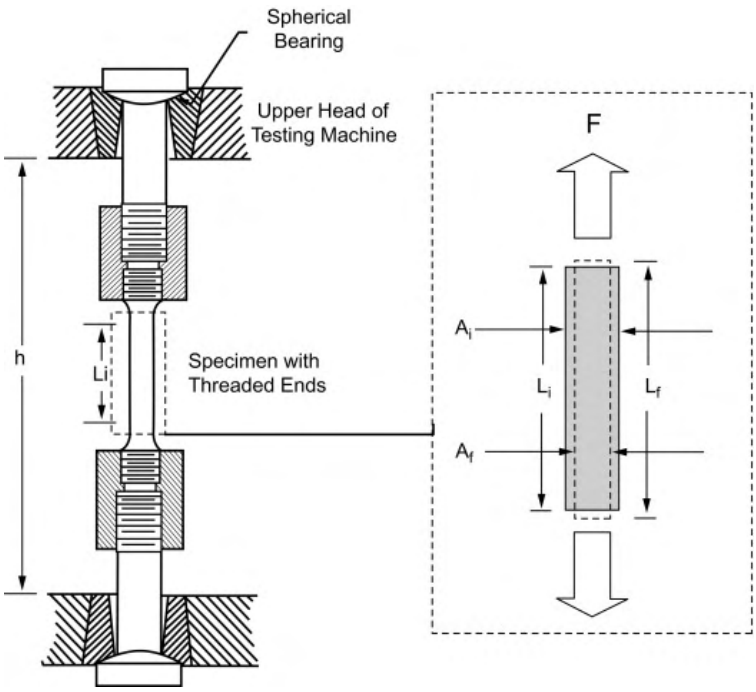

Figure 2.2: Schematic of Uniaxial Tension Testing [6]

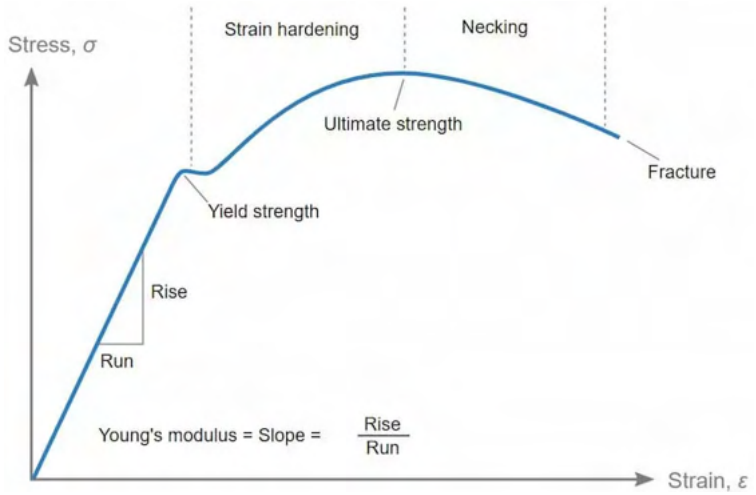

Figure 2.3: Enginnering Stress-Strain Curve Example [7]

The issue with using uniaxial tension tests results for the classification of a materials formability in pressing operations is that the tension is often not uniaxial [1]. As the name suggests, uniaxial stress is stress in one direction only (like in a tensile test) with the stress

in the other two orthogonal directions equal to zero. The major principal strain is in the same direction as the tensile load (and is calculated using the measured elongation of the test specimen) and for an isotropic material, the stains in the directions orthogonal to the major principal strain must be equal to each other [1]. By applying the constant volume condition:

$$\epsilon_1 + \epsilon_2 + \epsilon_3 = 0 \tag{1}$$

it is possible to show that

$$\epsilon_2 = \epsilon_3 = \frac{-\epsilon_1}{2} \tag{2}$$

In a general sheet forming process, plane stress is assumed, that is the membrane stresses (σ_1, σ_2) are non-zero, while the third perpendicular stress (in the sheet thickness direction) is assumed to be zero, $\sigma_3 = 0$ [1], see Figure 2.4.

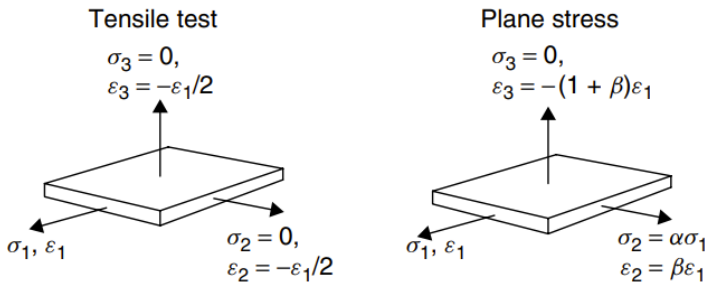

Figure 2.4: Stress Strain Condition For Tensile Test and Plane Stress Condition [1]

The ratio between the two membrane stresses and stains play a significant role in the outcome of sheet metal forming and are commonly referred to as α and β.

$$\alpha = \frac{\sigma_2}{\sigma_1} \tag{3}$$

$$\beta = \frac{\epsilon_2}{\epsilon_1} \tag{4}$$

Where, by convention σ_1 and ϵ_1 are the major principal stress and strain respectively and σ_2 and ϵ_2 are the minor stress and strain respectively, ($\sigma_1 > \sigma_2$ and $\epsilon_1 > \epsilon_2$) Applying the constant volume assumption the third principal strain (in the thickness direction) can be

obtained.

$$\epsilon_1; \qquad \epsilon_2 = \beta\epsilon_1; \qquad \epsilon_3 = -(1+\beta)\epsilon_1 \tag{5}$$

For uniaxial tension $\alpha = 0$ and $\beta = -\frac{1}{2}$

2.2.3 Deformation of sheets (modes)

The above section introduced β which is the ratio between the principal in plane strains ϵ_1 and ϵ_2. This value is useful for describing different modes of deformation in sheet metal forming. As $\epsilon_1 \geq \epsilon_2$, $\beta \leq 1$ for $\epsilon_1 \geq 0$, and in practice, $-2 \leq \beta \leq 1$, the table below gives an overview of the different deformation modes, and modes are illustrated in Figure 2.5.

β	Mode	Description
1	Equal Biaxial Stretching	The sheet is stretched equally in both directions as the membrane stresses are equal ($\alpha = 1$)
0	Plane Strain	The sheet only extends in the major principal direction
-1/2	Unixial Tension	The sheet is stressed in the major direction only ($\alpha = 0$), the sheet will stretch in one direction and contract in the other
-1	Drawing	Also known as constant thickness or pure shear, the membrane stresses and strains are equal and opposite
-2	Uniaxial Compression	An extreme case where $\sigma_1 = 0$ and $\sigma_2 < 0$, the sheet thickens and wrinkling is likely

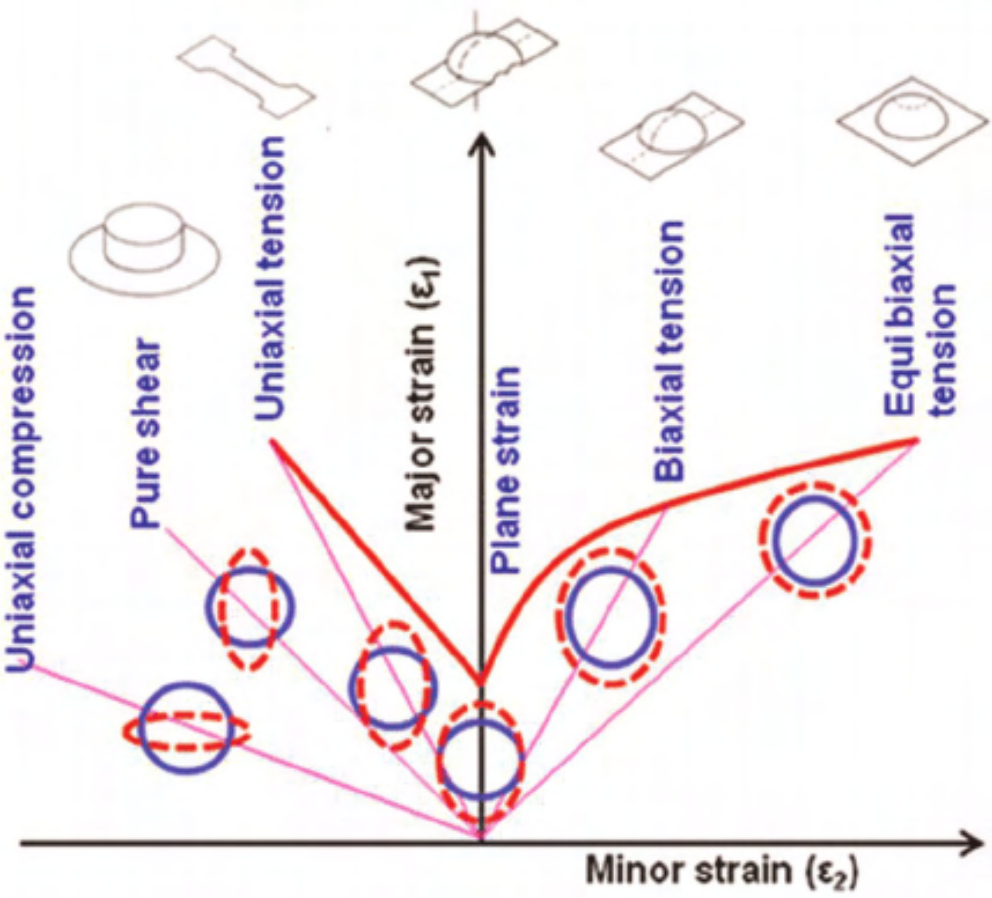

Figure 2.5: Strain State and Deformation Mode [8]

2.2.4 Forming Limit Diagram

The previous sections have outlined the processes for sheet metal deformation but there has been no consideration given to the limits of this deformation. Observation of a uniaxial stress strain curve highlights one form of deformation limits, necking. Ductile material under uniaxial tension will elastically deform upto the yield strength of the material (σ_y) at which point, plastic deformation will start and the stress and strain will continue to rise until the ultimate tensile strength of the material is reached, at which point the engineering stress will begin to decease and the strain will continue to increase until the material fails. The engineering stress reaches a maximum as diffuse necking develops in the material which reduces the cross section of the test specimen, reducing the load carrying capacity, and the

necking region continues to develop with the deformation concentrated within this region. These points are clearly seen in the engineering stress strain curve, Figure 2.3.

In a continuous sheet stretched over a punch, diffuse necking is not observed as the increased strain in the necking region would cause the sheet the move away from the punch, which is not possible. There have been a number of different models developed to predict the necking strain conditions for sheets. Hill 1952 [9] proposed that local necking will develop when the major tension reaches a maximum. Here tension refers to the force per unit width of the sheet, which is calculated from the current principal stress and thickness t. This theory put forward by Hill suggests there is a direct relationship between the onset of local necking and the strain hardening rate of the material. This theory shows good agreement with observations of low carbon steels when $\beta < 0$. Experimental results show that necking does occur when $\beta > 0$ and the strain state at the onset of necking exceeds the maximum tension line. Swift 1952 [10] modelled the occurrence of necking under biaxial stress ($\beta = 1$) by assuming necking is initiated by diffuse necking. Later in 1967 Marciniak and Kuczynski (MK) [11] developed a different theory to explain necking behaviour under biaxial tension. This theory is based on the assumption that there is a thickness imperfection band in the sheet that is perpendicular to the direction of σ_1 and that the strain parallel to this band is equal either side of the boundary of this band. The magnitude of this imperfection is characterized by the initial thickness ratio between the imperfection region and the uniform region referred to as the inhomogeneity factor;

$$f_0 = \left(\frac{t_{\text{imperfection}}}{t_{\text{uniform}}} \right)_0 \tag{6}$$

The predicted strain state for the onset of necking is therefore dependent on the assumed inhomogeneity factor, typically in the order of $(1 - f_0) = 0.001$. The MK theory predicts greater strains at the onset of necking when compared to Hill's theory for $\epsilon_2 > 0$, which agrees with experimental observations, and suggests there is some process that slows or stabilizes necking development when a sheet is under biaxial tension [1]. Both the Swift and MK theories perform better than the Hill theory when $\beta > 0$, with Swift generally under predicting and MK over predicted (Figure 2.6) the onset of necking stress state, and as shown

by [12] can be used as a lower and upper bound for predicting necking behaviour in sheet metal.

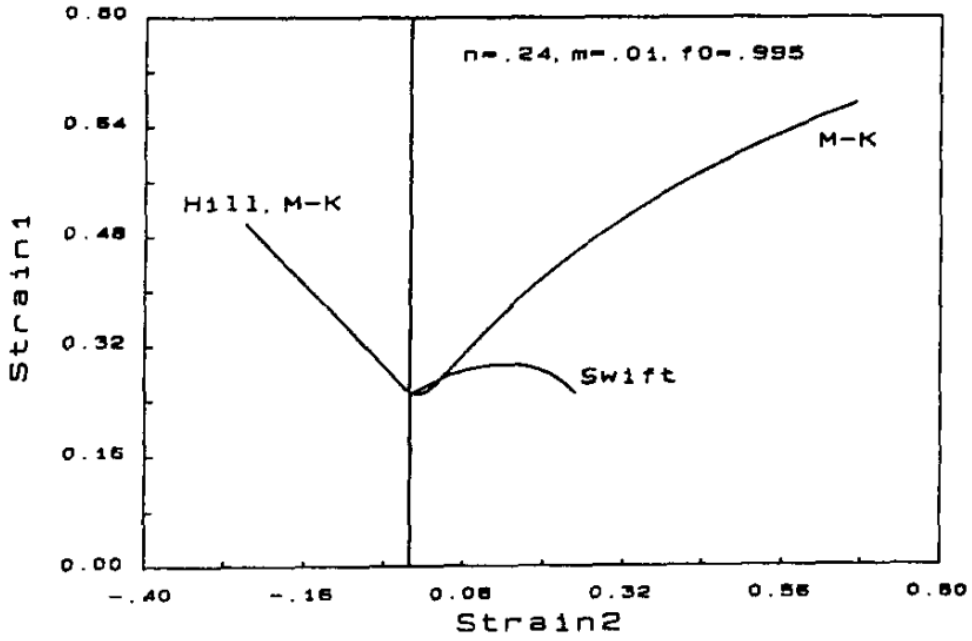

Figure 2.6: Forming Limit Curve Prediction [12]

2.2.5 Forming Limit Measurement

As seen in the previous section, the developed theories are able to predict trends and estimate forming limits, but due to the complex nature of forming and other factors such as deformation rate, material inhomogeneity, anisotropy, tribology, sheet thickness and galling, physical specimen testing is required to accurately quantify a materials forming limit. The concept of a Forming Limit Diagram (FLD) was developed by Keeler and Backhofen 1963 [13] and Goodwin 1968 [14] as a way to visually represent the different strain conditions at the point of fracture for different materials. A Forming Limit Curve (FLC), which divides the stress state into regions of safe forming and fracture, is experimentally determined and plotted on the FLD. ISO12004 was developed from the work of Nakajima et. al, 1971 [15] to standardize the experimental method used to determine the forming limits of sheet metal. The procedure involves stretching circular blanks cut to different widths over a cylindrical or

hemispheric punch until necking occurs. The difference in blank geometry creates different strain conditions, with the circular specimen approximating equal biaxial strain and the narrowest specimen approximating uniaxial tension. The FLC is created by joining these strain condition points, with a second 'safety' curve offset from the FLC to indicate an appropriated safety margin [1], see Figures 2.7 and 2.8.

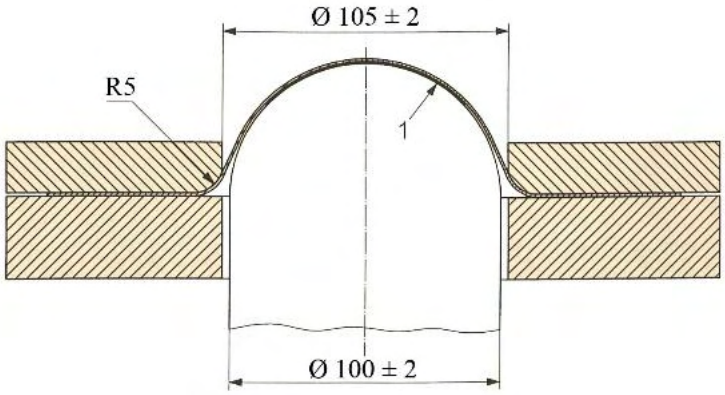

Figure 2.7: Schematic of Nakajima Forming Limit Test [16]

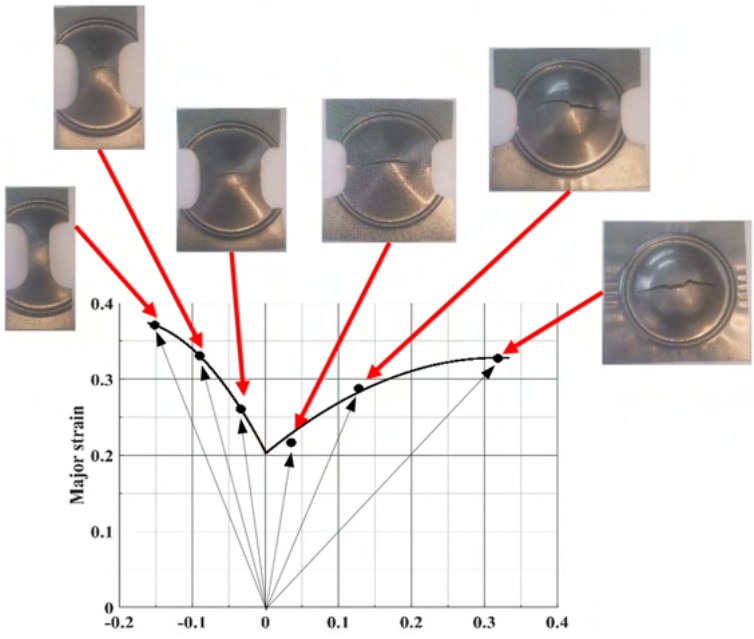

Figure 2.8: Test Specimens for Nakajima Forming Limit Test [17]

Issues with this test include difficulty in assessing whether or not acute necking has

occurred in the test specimen as the onset can be subtle and hard to define objectively as mentioned in a number of works such as, Cheong 2019 [18] and Isik et. al. 2014 [19]. Works by DiCecco et al. 2016 [20] have explored different ways to detect the onset of local thinning by monitoring the changes in the deforming surface curvature.

2.3 Lubrication and Galling During Forming Operations

As there is close contact, high pressing forces and relative material flow between the tool and the sheet metal, the tribological conditions during forming are an important factor in formability. Lubrication of the contact surface reduces frictional forces, allows for greater material draw and stretching and alters the location of the minimum sheet thickness [1], and therefore material and lubrication should be considered when determining formability.

Galling is a common phenomenon that is indirectly related to formability. Galling is the material transfer between contacting surfaces that occurs in sliding systems. In sheet metal forming, galling can occur when the soft sheet surface material is transferred to the hard tool surface as they slide over each other. The effect and mechanisms of the galling phenomenon during sheet metal forming is explored in a number of works. Bernick 1977 [21] conducted work in developing testing procedures for evaluating galling in sheet metal stretching and drawing operations, as existing adhesive wear tests were shown to be unsuitable for these operations. Their tests agreed with adhesive wear behaviour;

- The amount of wear is proportional to the applied normal load
- The amount of wear is proportional to the distance slid
- The amount of wear is inversely proportional to the hardness of the surface being worn

They found a strong link between the sliding frictional forces and galling tendencies, highlighting the role of lubricants during forming operations and go on to identify three key requirements for lubricants;

1. Ability to eliminate material pick-up and scoring

2. Promotion of the required surface finish

3. Ability to reduce friction and to promote formability

E.Schedin 1994 [22] and B. Lehtinen, Erik Schedin 1993 [23] investigated galling initiation and growth behaviour for a range of sheet material. Their results show that galling is initiated on the tool surface at locations of surface defects (e.g. grinding scratches introduced during tool manufacturing). They also concluded that the galling tendency is related to tool surface roughness, sheet surface finish and sheet hardness. They go on to suggest that surface chemistry also plays a role due to formation of hard oxide layers and chemical incompatibility between the sheet and the tool. Interestingly, they conclude that the initiation of galling is virtually insensitive to material and lubrication used, instead it is the growth rate (build up) of the lumps at the initiation sites that is dependent on the material and lubrication used.

Adhesion growth was further examined by Kitano and Dohda 2018 [24] who developed a model to predict the growth rate of adhesion occurrence on contact surface of the sheet metal and the die.

2.4 FEM

The use of Finite Element Method (FEM) to predict the sheet metal forming process is highly desirably in the punch and die design, as it can drastically reduce prototyping time and costs, as performance of different geometries can be accurately evaluated without physical manufacturing and testing. Due to the time and cost savings, FEM forming simulations is today widely used in the automotive and other sheet metal forming industries. Development in general FEM tools started in the 1960's, however, up until the early 1970's, forming simulations were considered to complicated for the current tools and computational power. The main complications of modelling the sheet metal forming process are; the non-linear behaviour of the material deformation, the complex contact conditions between the tool and part and the large strains developed during forming [25]. At the time, FEM formulations were well developed for predicted small strain behaviour, and were developed to describe the displacement of material at some point in time, known as the Lagrangian description. In

1970 Hibbitt et al. presented the first formulation for large strains based on the Lagrangian description, however, at the time solution for forming simulations were limited to plane-strain or axi-symmetrical cases only. Today programs like like LS-DYNA and ABAQUS use dynamic explicit codes and are widely used by industry for sheet stamping simulations. These tools are capable of simulating complex pressing geometries and can be used to predict strain states in formed sheet metal parts, which, when compared with known material FLCs can predict necking and fracture all before a single tool is manufactured.

2.5 Current Procedure Performed by Alfa Laval

In order to better replicate the forming operations used in the production of heat exchanger plates, material formability is evaluated using test pressings of small plates with features geometrically similar to those found in production rather than the standard cylindrical or hemispherical test pressings outlined by ISO12004. This has the advantage of better representing the stress and strain conditions experienced by the material on the production floor, and the effects of repeat pressing without cleaning the tool is better captured. The disadvantage is that the complex geometry of the test plate makes some analysis more difficult, the presents of necking and cracking is harder to predict and visual identification of forming defects can be difficult due to the complex geometry.

3 Method

This chapter will outline the following methods;

- The procedure followed to perform the pressing of the stainless steel (316L) and titanium (grade 1) test material,
- An overview of the current formability evaluation method including how material formability scores are calculated
- The steps followed to capture the material thickness data using 3D scanning

3.1 Pressing of Test Materials

The same procedure for pressing test material blanks is followed to minimise test error. The steps are as follows:

1. Pre cut blanks from the supplier are inspected for defects, dimensional tolerance and rolling direction is identified, see Figure 3.1

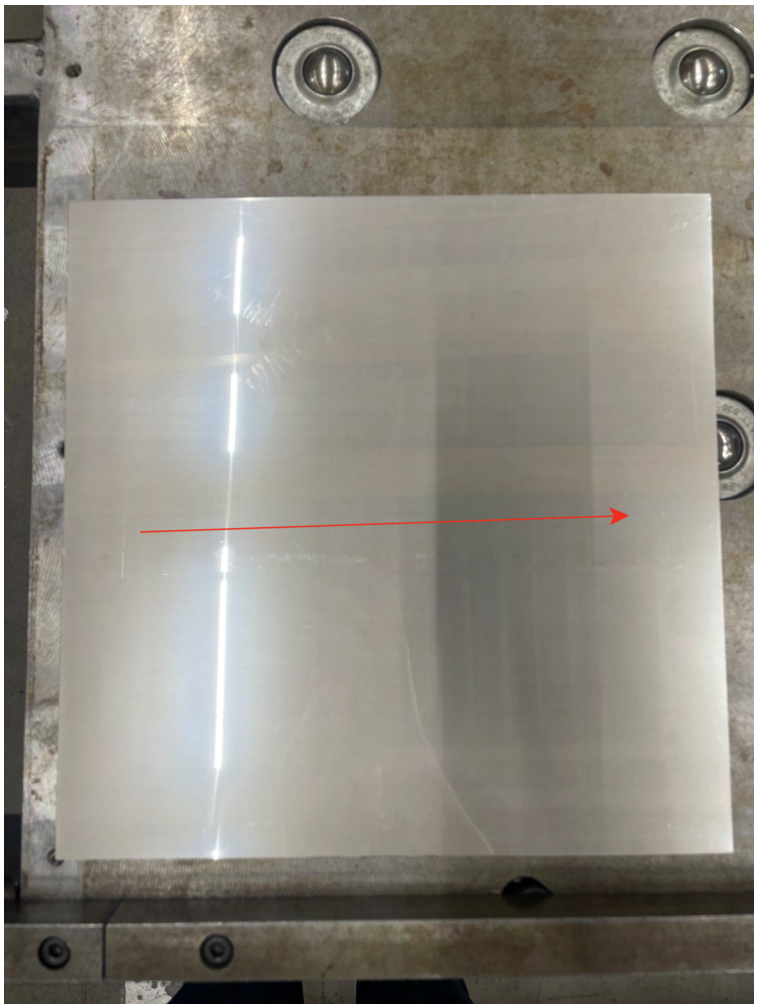

Figure 3.1: Stainless Steel 330 x 330mm Blank, Arrow Indicates Rolling Direction

2. Blanks are engraved with heat number and press number to keep track of test results

3. Once the pressing tool has been loaded into the press (as shown in Figure 3.2) it is cleaned to remove old lubricant and surface contaminants

Figure 3.2: Tool Loaded in Press, Arrow Indicates In-Feed Direction

4. To remove any adhered material on the tool (which can occur during titanium material testing) and to ensure the tool is well lubricated, 5 stainless steel blanks are pressed and then discarded

5. Lubrication is applied directly and to both side of the blanks using a roller, the same lubricant is used for each test material

6. Blanks are loaded into the press with material rolling direction parallel to the in-feed direction, see Figure 3.2

7. Blanks are pressed with the same pressure and cross head speed

8. Press plates (see Figure 3.3) are removed from the tool, washed to remove lubricant and stored for later analysis

Figure 3.3: Titanium Pressed Plate

9. Steps 5-8 are repeated depending on the test material (5 times for 316L test material and 25 times for titanium test material)

3.2 Visual Evaluation Method

Once the pressing for a test material has been completed, the standard visual formality evaluation method is performed. The steps are as follows:

1. The 15 standard evaluation points are located and the surface is marked

2. In a well lit environment, trained technicians visual inspect and evaluate the material surface at the marked evaluation points

3. Each evaluation point is assigned a scored, depending on the presence and type of surface defect, 0 = Large Crack, 1 = Small Crack, 2 = Necking, 3 = Necking Tendency, 4 = No Surface Defect. See Figure 3.4 for examples of scores

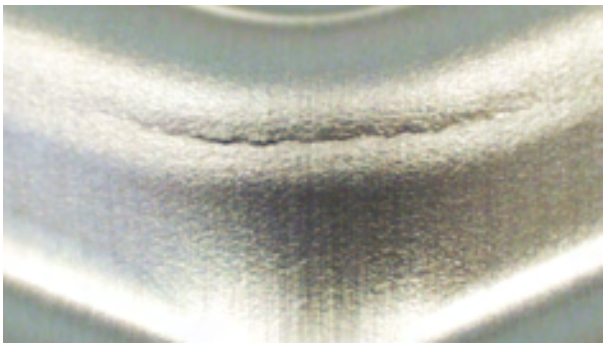

(a) Small Crack, Score = 1

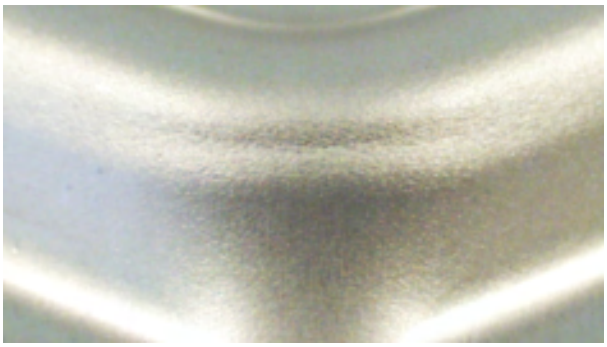

(b) Necking Score = 2

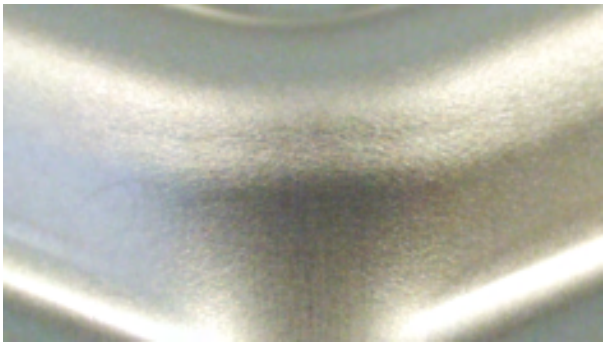

(c) Necking Tendency Score = 3

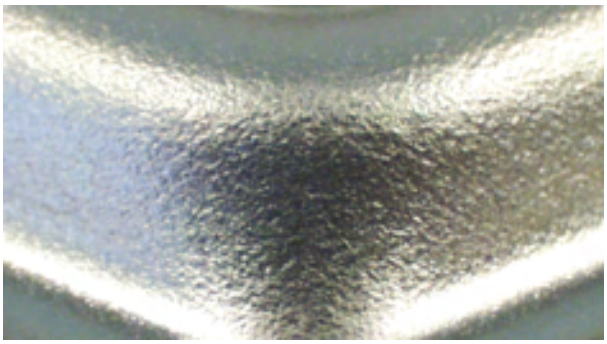

(d) No Surface Defect Score = 4

Figure 3.4: Evaluation Point Scoring Example

4. The individual scores at each evaluation point are added together and expressed as a percentage of the maximum score (60)

5. Steps 2-4 are repeated by 2 other technicians and the total scores are averaged

3.3 Scanning

After completing the visual evaluation of the test material, select pressed plates were chosen for 3D scanning. The steps are as follows:

1. Due to the high reflectivity of the test material, a thin layer (approximately $10\mu m$) of specially formulated matt scanning paint is applied to each surface
2. The coated plates are installed in a vertical fixture, which has fixed reference points
3. After calibration, laser scanning is to capture a cloud of points on one surface, multiple scans are completed from different positions and angles to capture the whole area of the plate and to capture details with steep surface angles
4. The fixture is rotated and the other surface is captured
5. Using both point clouds and the reference points on the fixture, a surface mesh that represents the plate is created
6. The mesh is refined and parts of the fixture are removed, see Figure 3.5
7. Using the computed surface mesh, the surface normal distance between mesh points is calculated to obtain the material thickness over the entire plate, see Figure 3.5

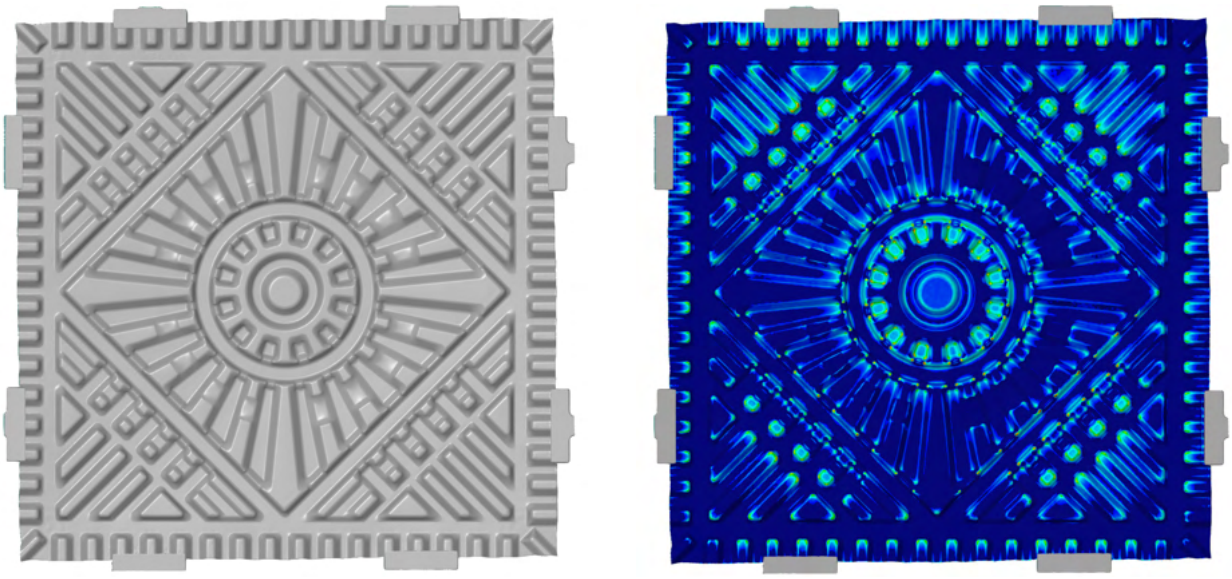

(a) Surface Mesh of Plate from Scanning

(b) Computed Material Thickness

Figure 3.5: 3D Scan Measurements

4 Results

4.1 Visual Evaluation

The formability of the pressed plates were determined using the existing visual evaluation procedure. The scoring of each evaluation point was repeated by 3 trained technicians.

4.1.1 Pressing Summary

A total of 55 316L blanks from 7 heats and 125 Titanium blanks from 5 heats were pressed using the same procedure and lubricant. Table 4.1 presents a summary of all the pressings.

Material	Supplier	Heat	Press Date	Number
316L	A	1	2023-02-01	25
316L	A	2	2023-02-07	5
316L	A	3	2023-02-27	5
316L	B	1	2023-02-27	5
316L	B	2	2023-02-27	5
316L	B	3	2023-02-27	5
316L	A	4	2023-02-27	5
Ti(Gr1)	C	1	2023-02-28	25
Ti(Gr1)	C	2	2023-02-28	25
Ti(Gr1)	C	3	2023-02-28	25
Ti(Gr1)	C	4	2023-03-02	25
Ti(Gr1)	D	1	2023-03-06	25

Table 4.1: Test Pressing Summary

4.1.2 Visual Inspection Results

Using the current evaluation method, the first and last pressing from each 316L pressing event and pressings 1,3,5,10,15 and 25 from each titanium pressing event were evaluated.

Tables 4.2 and 4.3 present a summary of the average measured total score.

Supplier-Heat	First Score	Last Score
A1	92	97*
A2	98	92
A3	98	98
B1	95	98
B2	92	93
B3	98	98
A4	98	97

Table 4.2: 316L Visual Inspection Scores (* score of 25th pressing)

Supplier-Heat	#1	#3	#5	#10	#15	#25
C1	95	92	85	83	83	82
C2	90	90	90	87	83	82
C3	87	91	83	80	80	80
C4	78	68	63	63	63	60
D1	95	87	85	83	82	81

Table 4.3: Ti Average Total Visual Inspection Scores

The average and measurement variation of the total visual inspection score for each of the evaluated titanium plates is plotted as a function of press number in Figure 4.1.

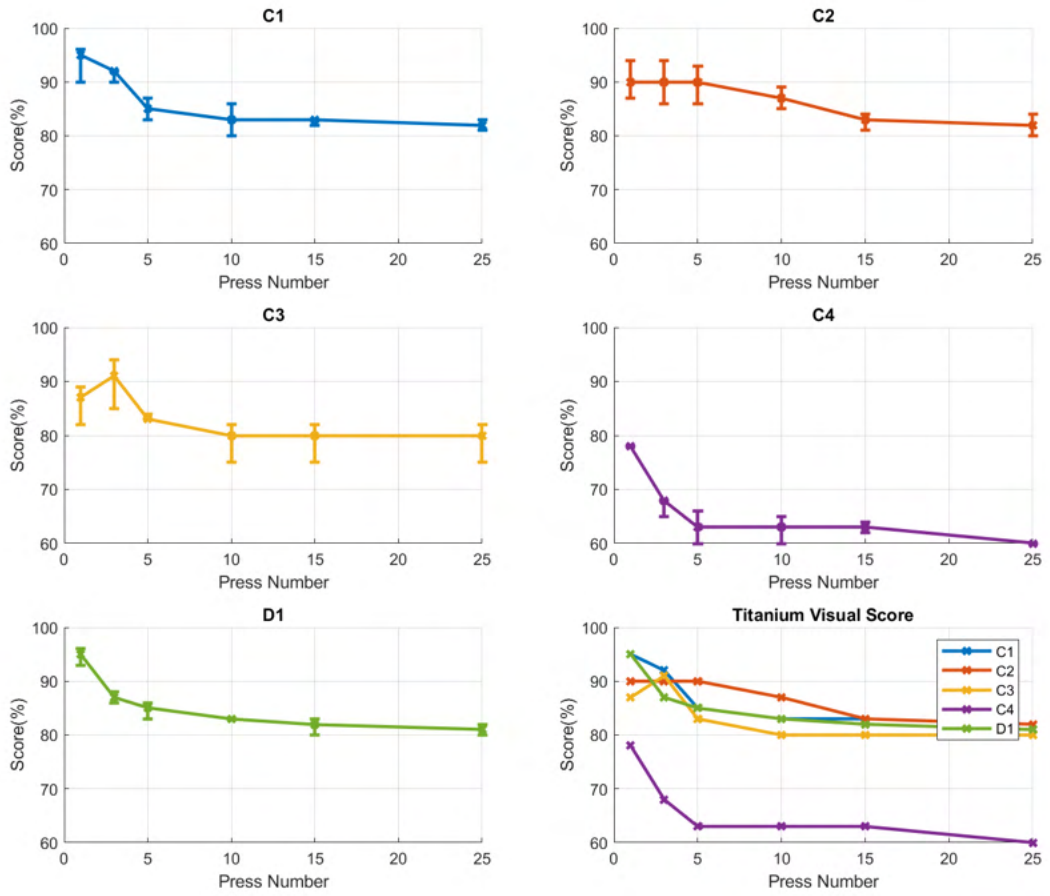

Figure 4.1: Titanium Visual Inspection Score vs Pressing Number

The 316L heats has a higher formabilty score compared to the titanium heats, and formability of the 316L heats is not dependent on press number, unlike the titanium heats where a negative trend is observed. These results are consistent with previous observations.

4.2 Scanning Results

After the visual evaluation had been completed, pressed plates were selected for scanning. Due to time limitations and the time required to complete one scan, only a limited number of plates were selected for scanning. A total of 8 plates were scanned. 2 316L heats and 2 titanium heats were selected in order to compare different materials and different heats of the same material. The heats were selected to try and maximise the range of scores to ensure a wide variety of surface defects could be analysed. This was difficult for the 316L heats as there was little variation in the total formability score, heats A1 and A2 were selected. For the titanium heats, heat C4 was an obvious choice as it formability performance is clearly poorer than the other heats. C1 was selected as the other titanium heats. The first and last pressing of each heat were both selected to compare the effects of press number. Table 4.4 summarises the plates selected for scanning and the used naming convention.

Name	Material	Heat	Press #
A1#1	316L	A1	1
A1#25	316L	A1	25
A2#1	316L	A2	1
A2#5	316L	A2	5
C4#1	Ti	C4	1
C4#25	Ti	C4	25
C1#1	Ti	C1	1
C1#25	Ti	C1	25

Table 4.4: Scanned Plates Summary

Figures 4.2 and 4.3 presents the material thickness for the first pressings of the 316L and titanium heats respectively.

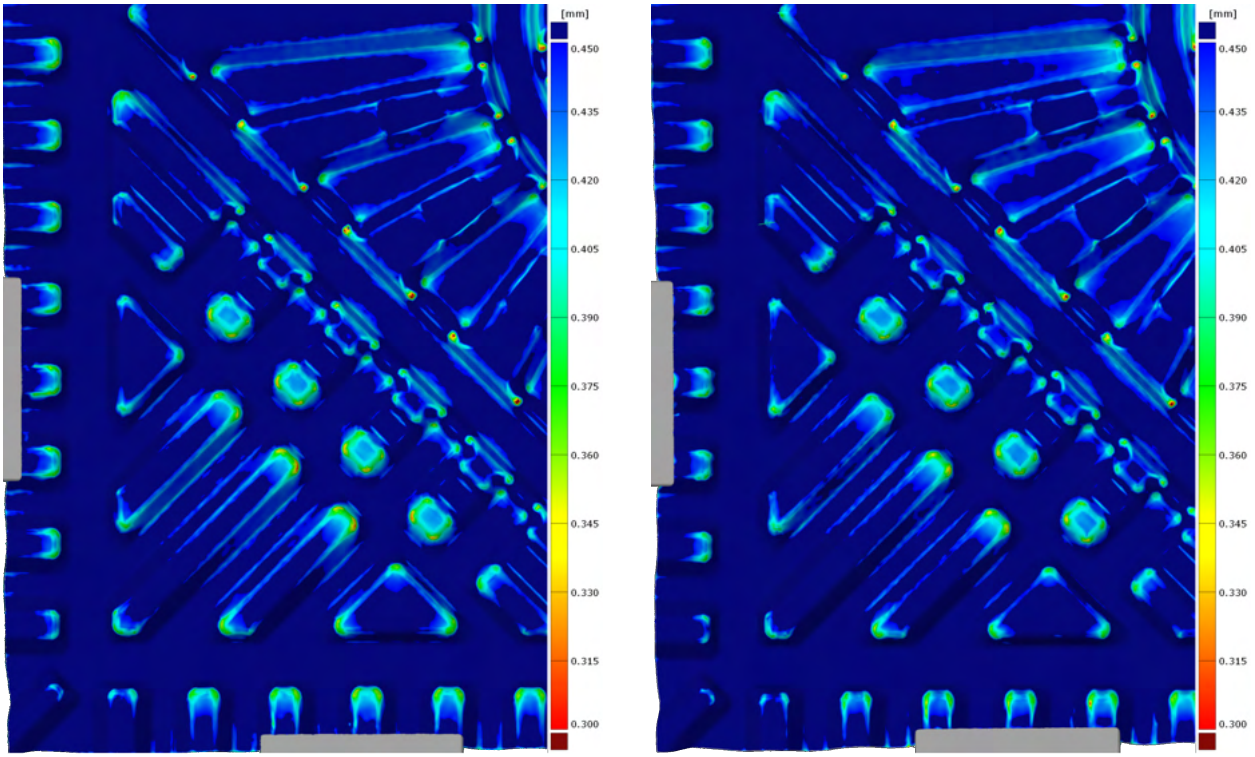

(a) A1 #1

(b) A2 #1

Figure 4.2: 316L 3D Scan Results, Material Thickness

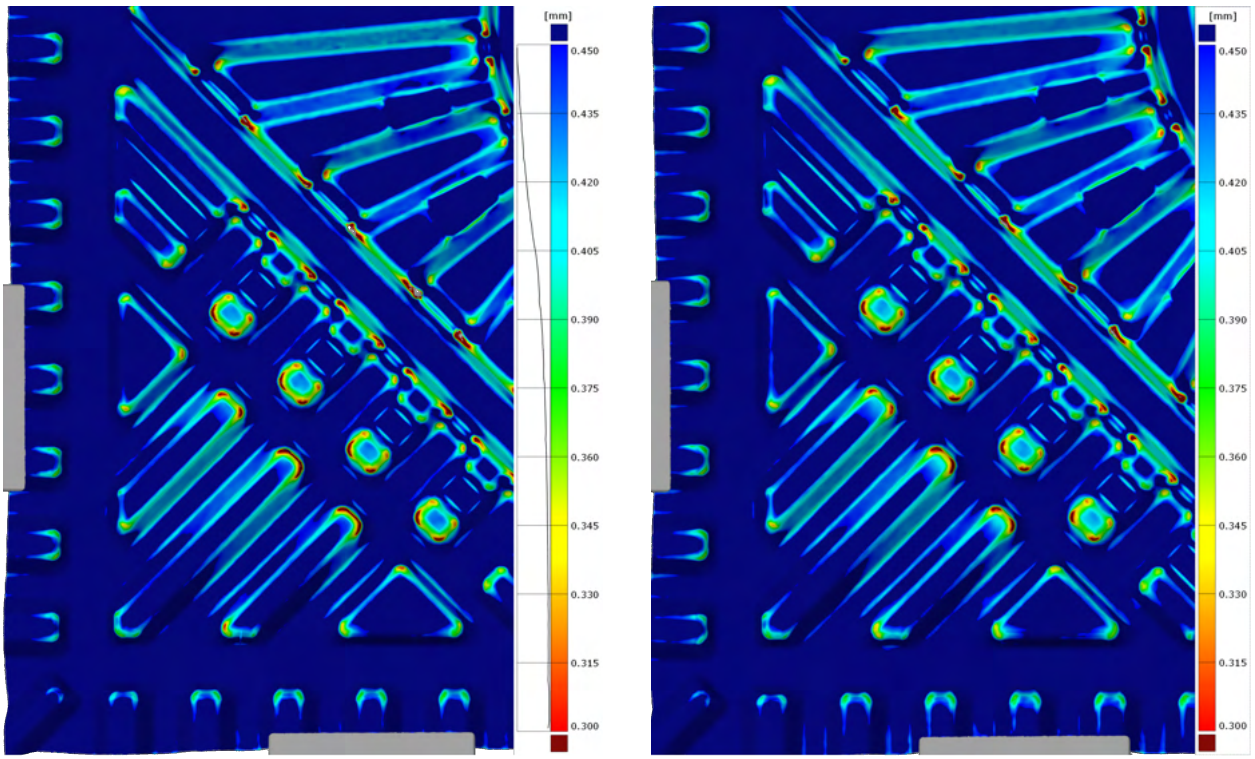

(a) C4 #1

(b) C1 #1

Figure 4.3: Ti 3D Scan Results, Material Thickness

From the above Figures a clear difference in the material thickness can be seen between the 316L heats and the titanium heats, with more material thinning observed in the titanium heats, which is expected as the titanium heats have lower formability scores.

4.2.1 Thickness Profile at Evaluation Points

Material thinning at the evaluation points was investigated by constructing line segments at the evaluation point passing through the point of minimum thickness and plotting the plate thickness along this segment. Figure 4.4 presents an example of a line segment and the thickness profile for evaluation point 1, to make comparison between different line segments easier, the segment position has been shifted so the at the minimum thickness is at segment position 0mm.

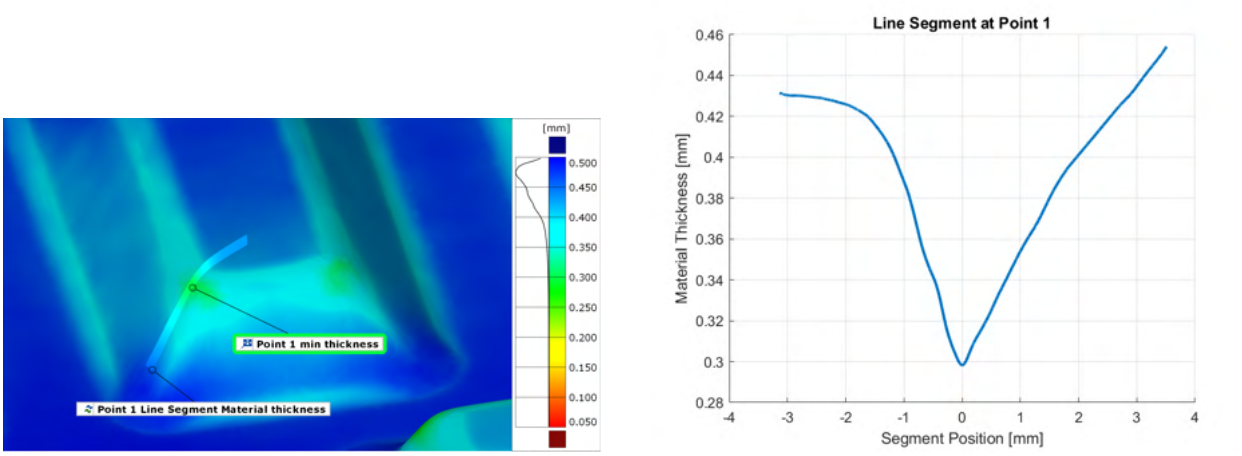

(a) Line Segment at Evaluation Point 1

(b) Material Thickness Profile Over Line Segment

Figure 4.4: Line Segment at Point 1 on Plate C1 #1

316L Thickness Profile

The thickness profiles for the 15 evaluation points, for the 316L heats are presented in Figure 4.5. Each profile has been coloured according to the visual score determined during the visual formability evaluation.

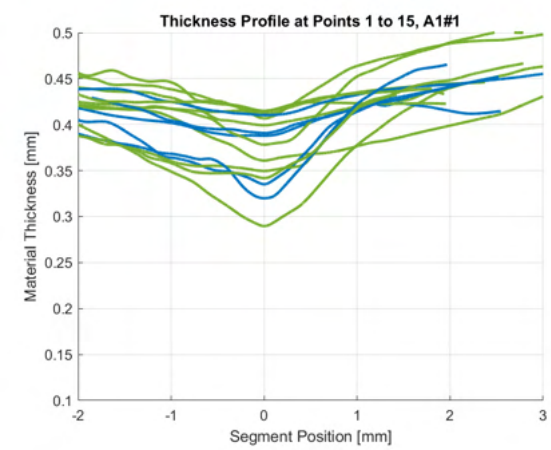

(a) A1 #1

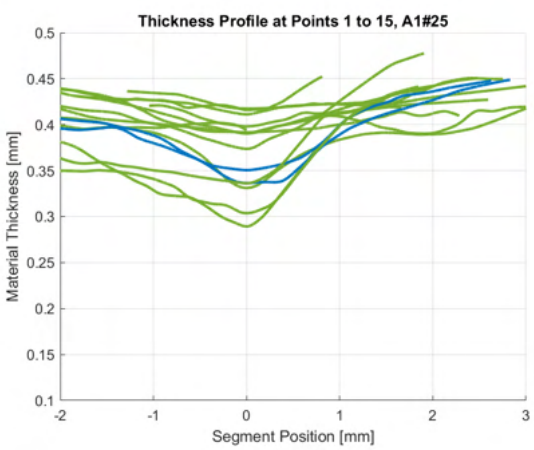

(b) A1 #25

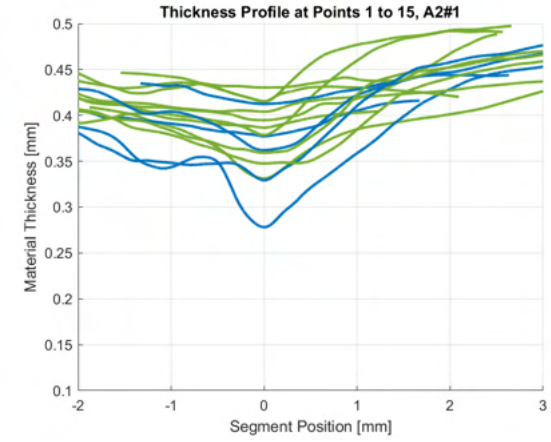

(c) A2 #1

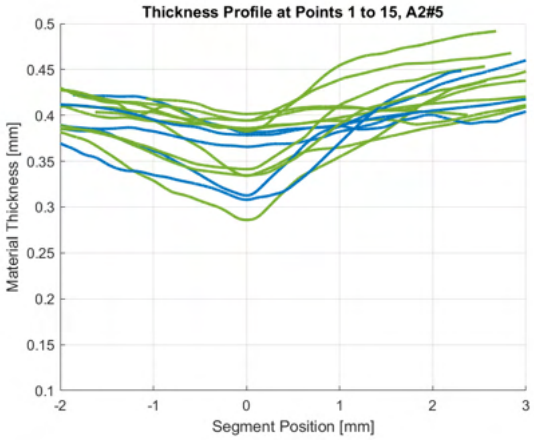

(d) A2 #5

Figure 4.5: Thickness Profiles At Evaluation Points, 316L, (Green = Good(4), Blue = Shadow(3), Yellow = Necking(2), Red = Crack(1))

Titanium Thickness Profile

The same analysis is repeated for the 4 titanium plates at the 15 evaluation points.

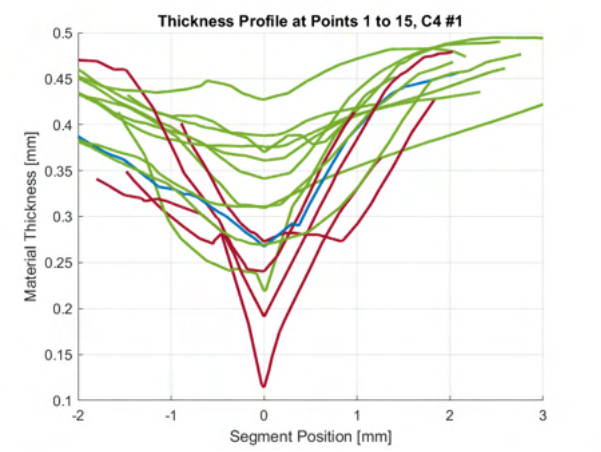

(a) C4 #1

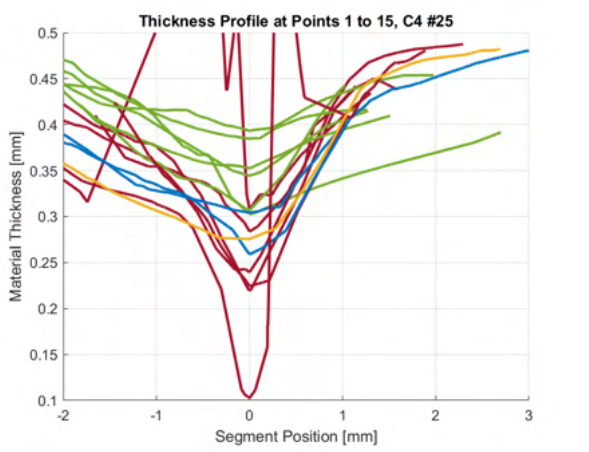

(b) C4 #25

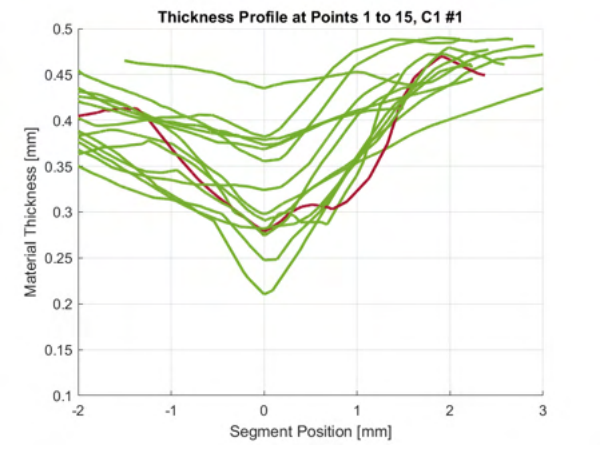

(c) C1 #1

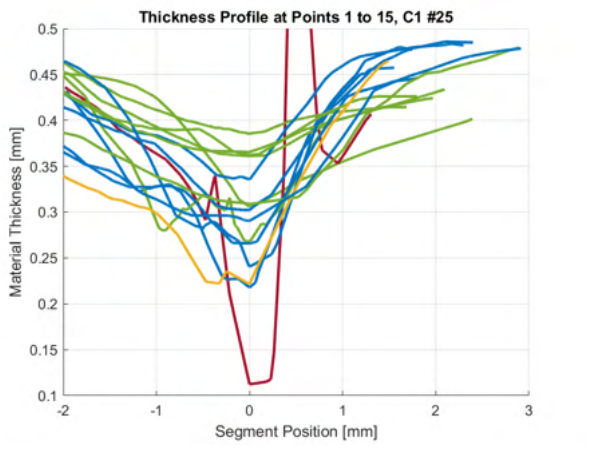

(d) C1 #25

Figure 4.6: Thickness Profiles At Evaluation Points, Ti, (Green = Good(4), Blue = Shadow(3), Yellow = Necking(2), Red = Crack(1))

4.2.2 Minimum Thickness

The minimum thickness for each evaluation point,(used to construct the line segments in the above section), is defined as the minimum thickness within small area that surround the point. Figure 4.7 presents an example of one such area.

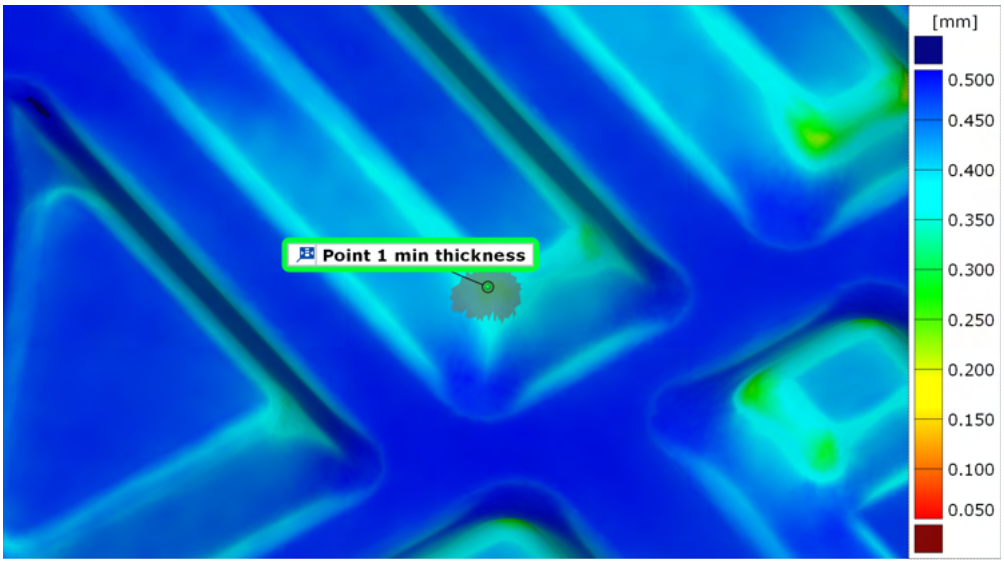

Figure 4.7: Evaluation Point 1 Minimum Thickness Search Area

316L Minimum Thickness

The minimum thickness for each evaluation point is plotted against visual score for the 4 316L plates in Figure 4.8.

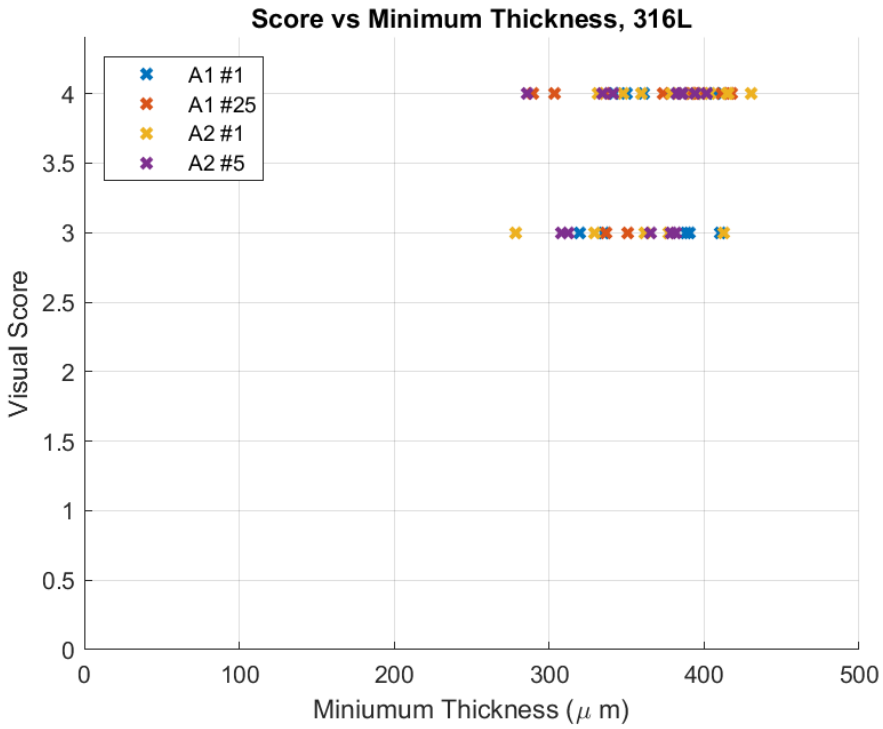

Figure 4.8: Visual score and Minimum thickness for scanned 316L Plates

Titanium Minimum Thickness The minimum thickness for each evaluation point is plotted against visual score for the 4 titanium plates in Figure 4.9.

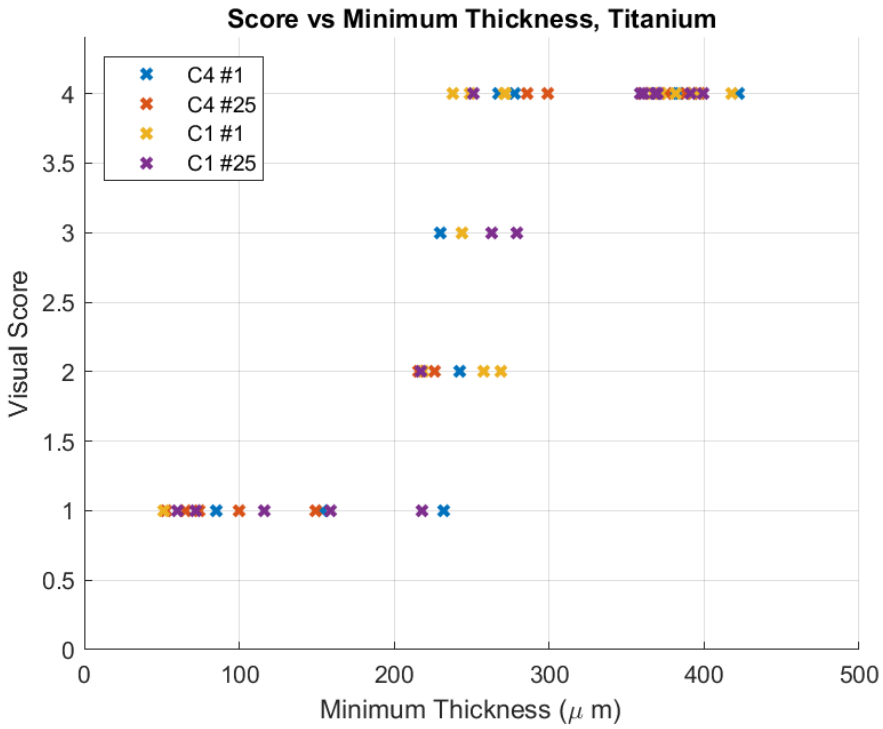

Figure 4.9: Visual score and Minimum thickness for scanned Titanium Plates

Figure 4.10 presents the average minimum thickness and standard deviation for each score, for each press individually.

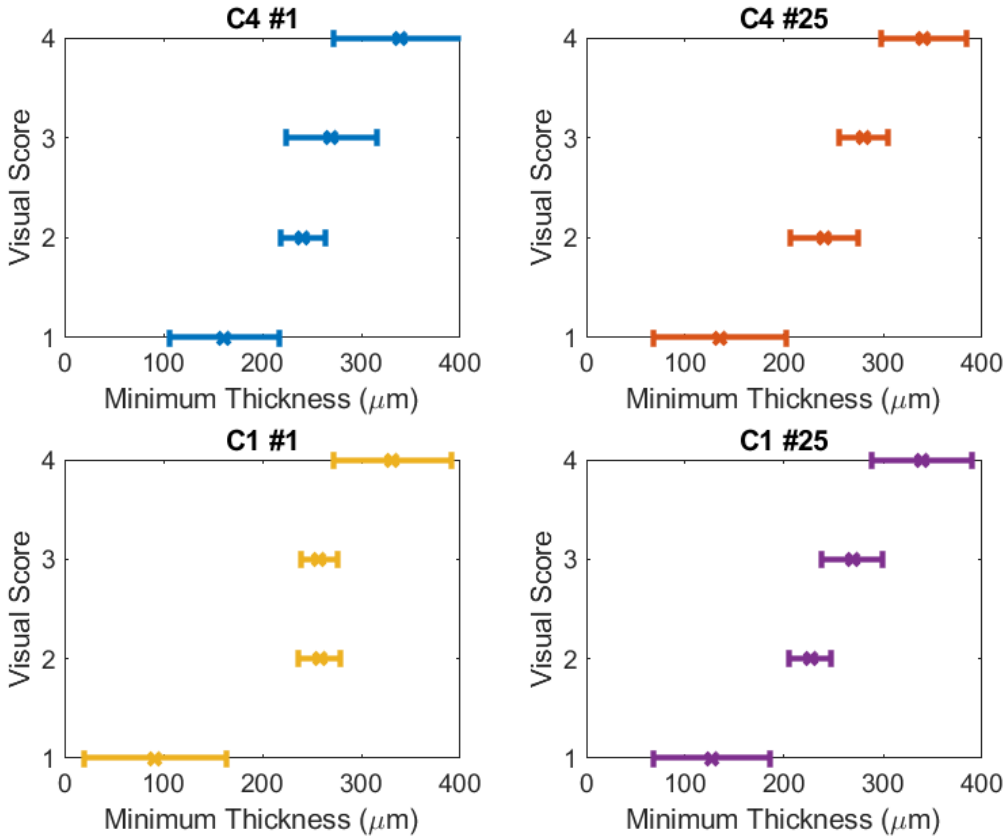

Figure 4.10: Visual score vs Minimum Thickness Average and Standard Deviation

4.2.3 Maximum Thickness Gradient

Necking causes material thinning to occur in small area, resulting in sharp changes in thinning behaviour. To better visualize these changes, the thickness gradient is computed over each evaluation point segment using a moving average to smooth out peaks. Figure 4.11 presents an example of a computed thickness gradient.

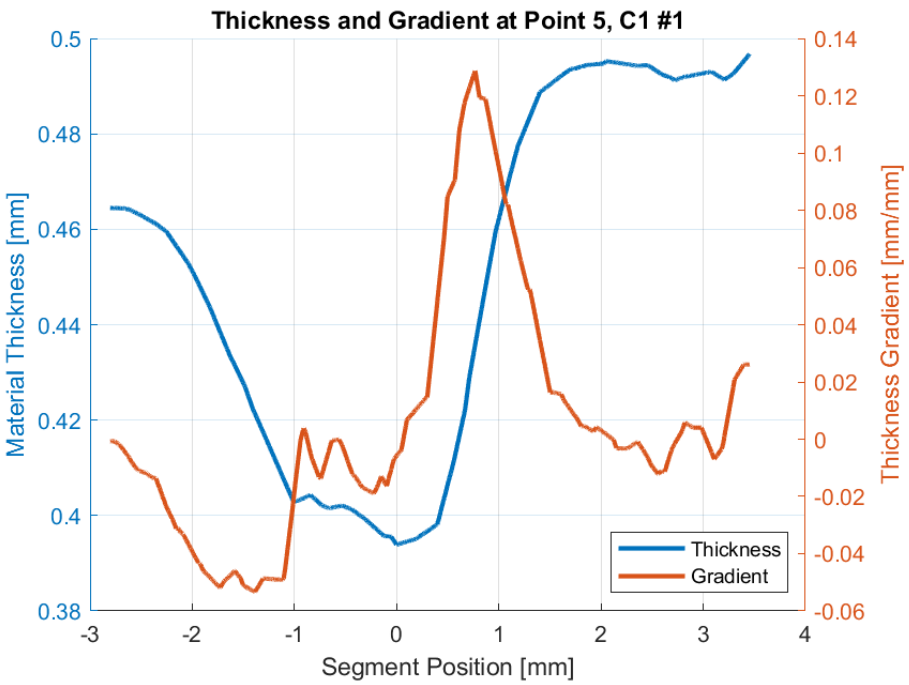

Figure 4.11: Example Material Thickness and Thickness Gradient

The maximum thickness gradients are compute and compared to the visual score for each evaluation point.

316L Maximum Thickness Gradient

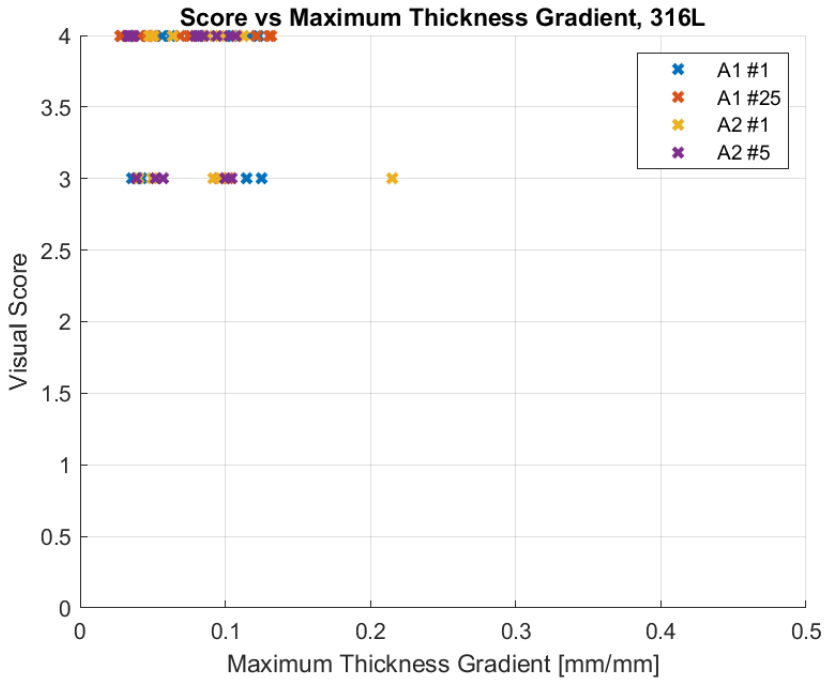

Figure 4.12: Relationship Between Maximum Thickness Gradient and Formability Score, 316L

Titanium Maximum Thickness Gradient

The maximum gradient magnitude for each evaluation point is calculated and plotted against formability score in Figure 4.13 for the 4 titanium plates.

Figure 4.13: Relationship Between Maximum Thickness Gradient and Formability Score

Figure 4.14 presents the average maximum gradient and standard deviation for each score, for each press individually.

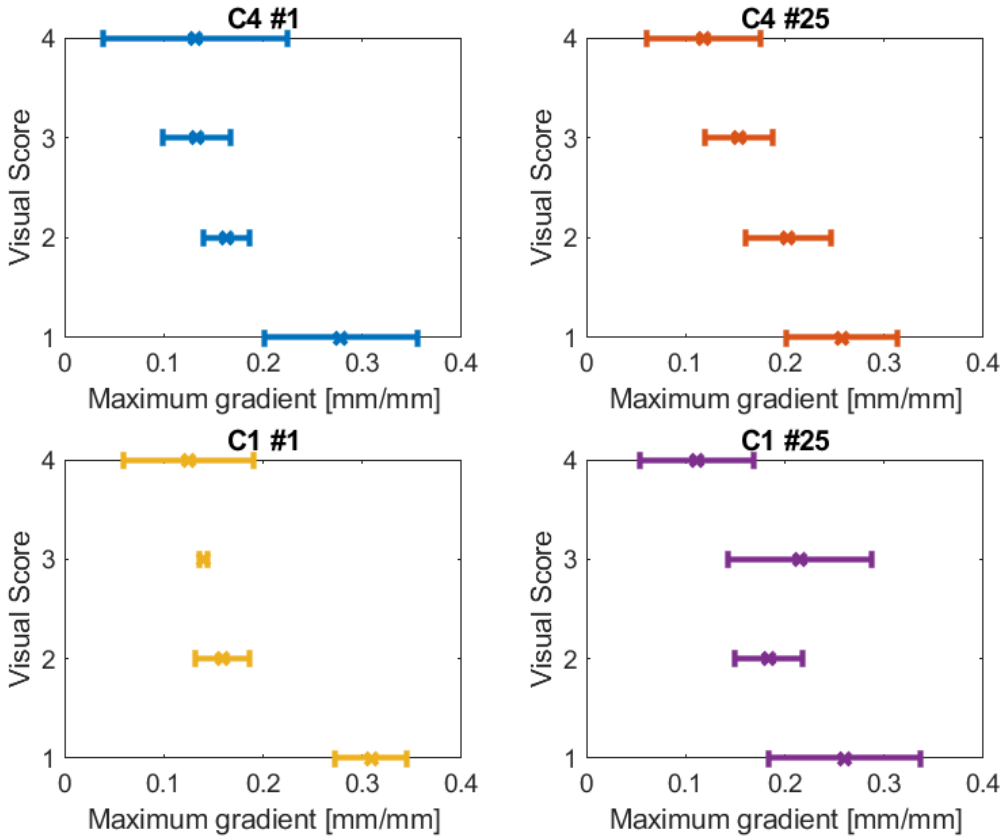

Figure 4.14: Visual Score vs Maximum Gradient Average and Standard Deviation

4.3 Strain State Estimation

The influence of the different evaluation point geometry on the strain state was investigated using a forming simulation. Results for 316L and titanium are very similar, only results for titanium are presented in this chapter. Figure 4.15 presents the results of a forming simulation for a generic titanium grade 1 heat. The results represent the strain state over the surface, areas are coloured based on the generic FLC presented in Figure 4.16.

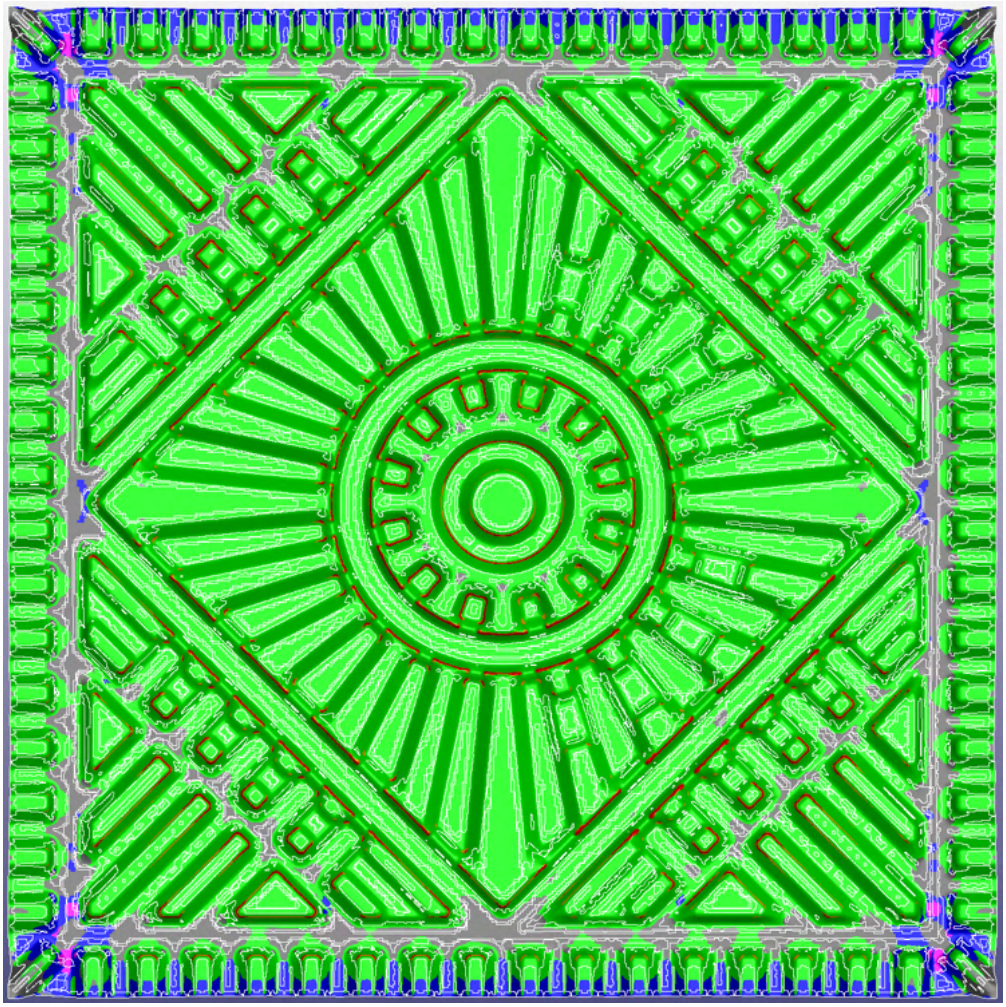

Figure 4.15: TI

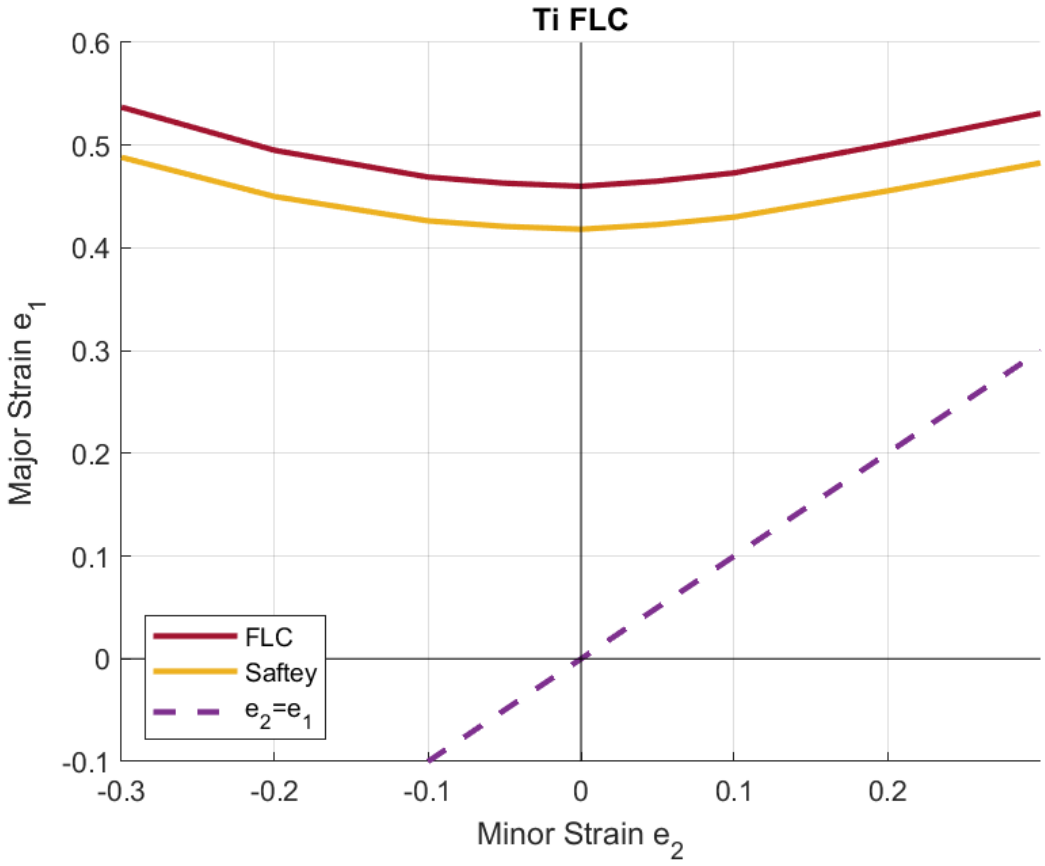

Figure 4.16: Titanium FLC

Strain state element points at evaluation points were selected to approximate the line segments constructed to analysis the thickness data in the section above. Figure 4.17 presents an example of points selected in the simulation results compared to the line segment constructed in the 3D scanning results.

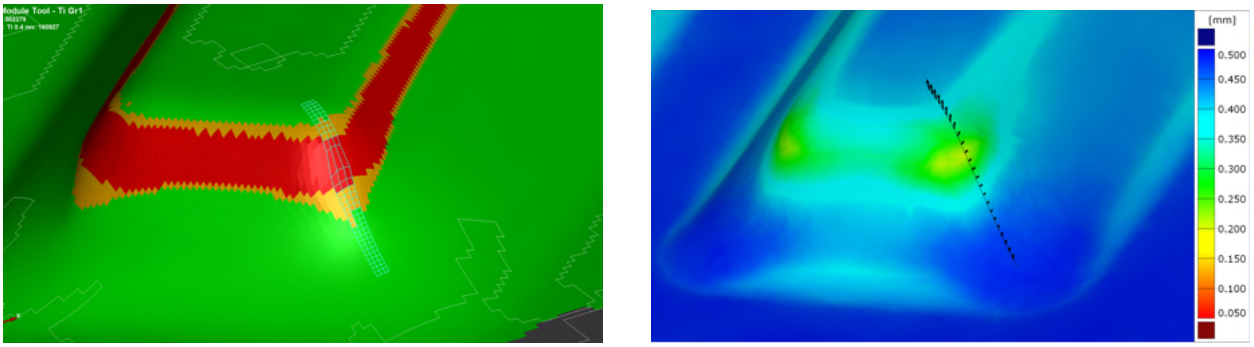

(a) Simulation Line Segment

(b) 3D Scanning Line Segment

Figure 4.17: Comparison Between Simulation and 3D Scan Segments at Evaluation Point 2

The strain state at each element point was plotted on an FLD, and repeated for all 15 evaluation points. Figure 4.18 presents an example of the strain state at evaluation point 2.

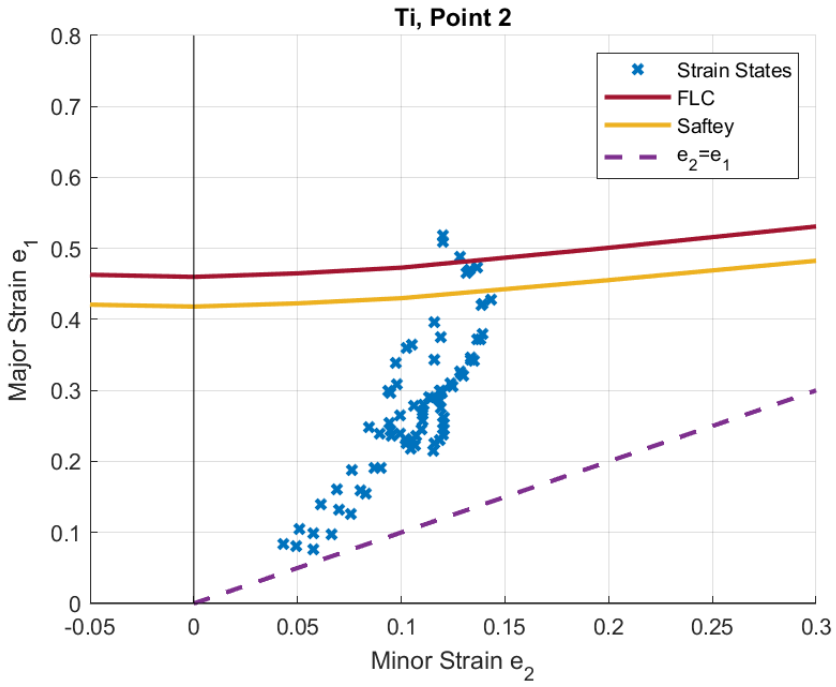

Figure 4.18: Strain State at Evaluation Point 2, Titanium

Figure 4.18 shows the stain state at point 2 increasing from a low strain state $\epsilon_1 \approx 0.1$ (outside of the bend) to a high strain state (within the bend) $\epsilon_1 \approx 0.5$, then returning to the

low strain state. The maximum strain state, ϵ_1 and ϵ_2 is extracted for all evaluation points for analysis in the next chapter

4.3.1 Titanium Strain State at Evaluation points

Table 4.5 presents maximum major and minor principal strains for each point for titanium.

Point	ϵ_1	ϵ_2	β
1	0.509	0.120	0.24
2	0.521	0.118	0.23
3	0.451	0.297	0.66
4	0.393	0.287	0.73
5	0.382	0.116	0.30
6	0.480	0.011	0.02
7	0.331	0.037	0.11
8	0.272	0.086	0.31
9	0.568	0.030	0.05
10	0.342	0.210	0.61
11	0.661	0.156	0.24
12	0.186	0.016	0.09
13	0.592	0.159	0.27
14	0.492	0.181	0.37
15	0.488	0.161	0.31

Table 4.5: Evaluation Point Approximate Principal Strains, Titanium

As expected the forming simulation predicts positive minor strains at all evaluation points. There exists a wide range of strain ratios, $0.02 \leq \beta \leq 0.73$. As the β ratio has an influence on how much material thinning can occur before surface defects occur, the thickness results are analysed again in conjunction with the strain state results in the next chapter.

4.4 Results Summary

This chapter presented the following results:

- the visual inspection scores for selected 316L and titanium plates,
- the pressed plate width measurements,
- the material thickness and thickness profiles at evaluation points obtained from 3D scanning for selected 316L and titanium plates
- the strain state data at each evaluation point extracted using a forming simulation for both 316L and titanium.

5 Discussion

5.1 Formability Score

The variation in measured total formability score highlights the subjective nature of the current evaluation procedure. Although the variation exists for both 316L and titanium evaluation results, the issue is easier to identify in titanium heats due to the wider and lower distribution of formability score. A major cause of this variation comes from the difficulty in visually assessing points with surface defects that are not cracks (i.e. 2s and 3s). This partly explains why the variation in 316L heats is lower, as a large majority of evaluation points are 4s, with the remainder being 3s. This also explains why lower scoring titanium heats tend to have lower variations as well, as lower scoring heats have a higher proportion of cracks (1s), which are easy to identify. Figure 5.1 presents an example of an evaluation point where recorded measurements differed between 2 and 3 depending on who performed the evaluation. It is clear that there is a surface defect at this evaluation point, however with an unaided eye it is difficult to classify the degree of the defect.

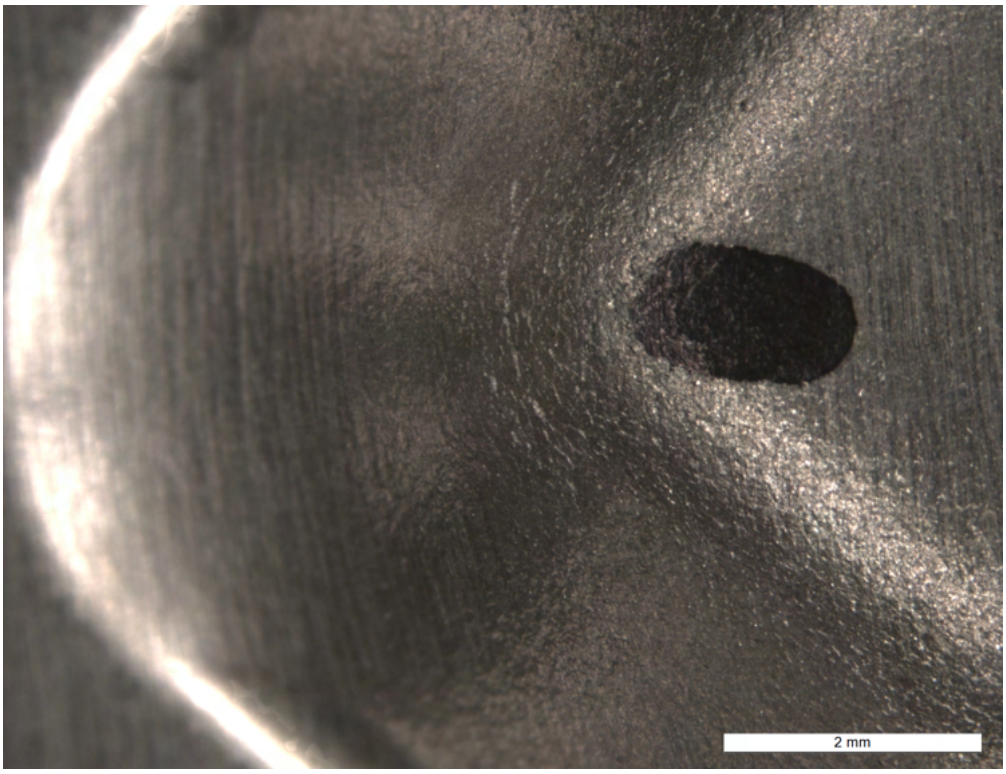

Figure 5.1: Evaluation Point 11, C1 #3

5.1.1 316L

An obvious issue when it comes to analysing the formability of 316L is the low variation in evaluation point scores for the tested heats. As seen in the histogram in Figure 5.2, all the evaluation points scores for the 14 evaluated plates are either 3s or 4s. This is the expected trend as the formability of 316L heats is almost always higher than titanium heats.

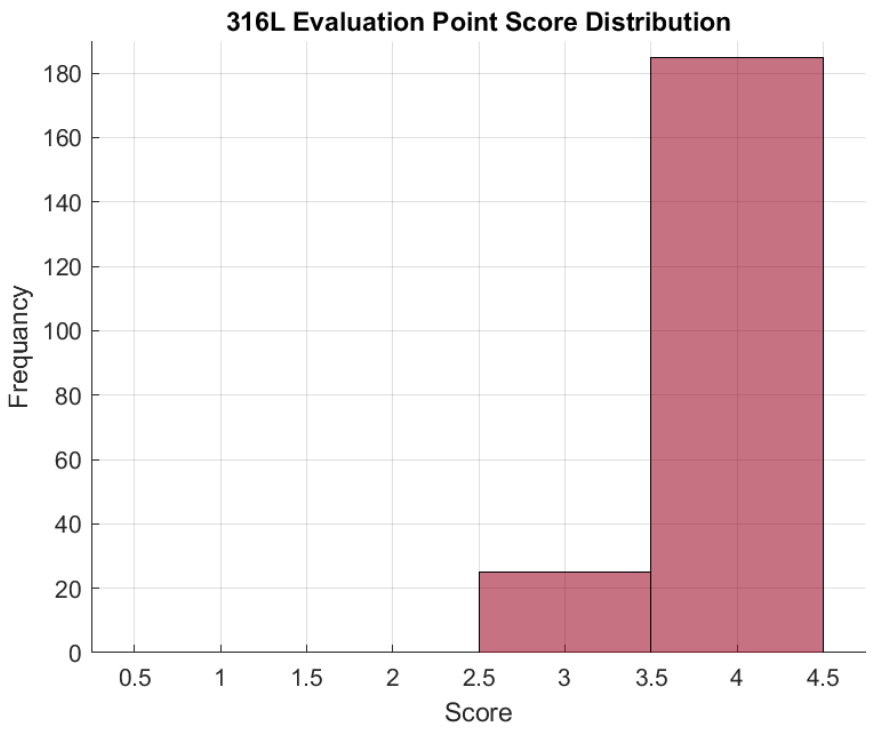

Figure 5.2: Distribution of Evaluation Scores, 316L

The low variation has made it difficult to detect trends between the scan data and the evaluation point score. Much of the analysis will therefore focus on the results from the titanium heats, with a general comparison between the two materials made at the end of this chapter.

5.1.2 Titanium

Unlike 316L, there is a good degree of variation of evaluation point scores for the titanium heats, as shown in the histogram if Figure 5.3. This variation allows for further analysis and relations to be made between the material thickness and the visual scores at evaluation points.

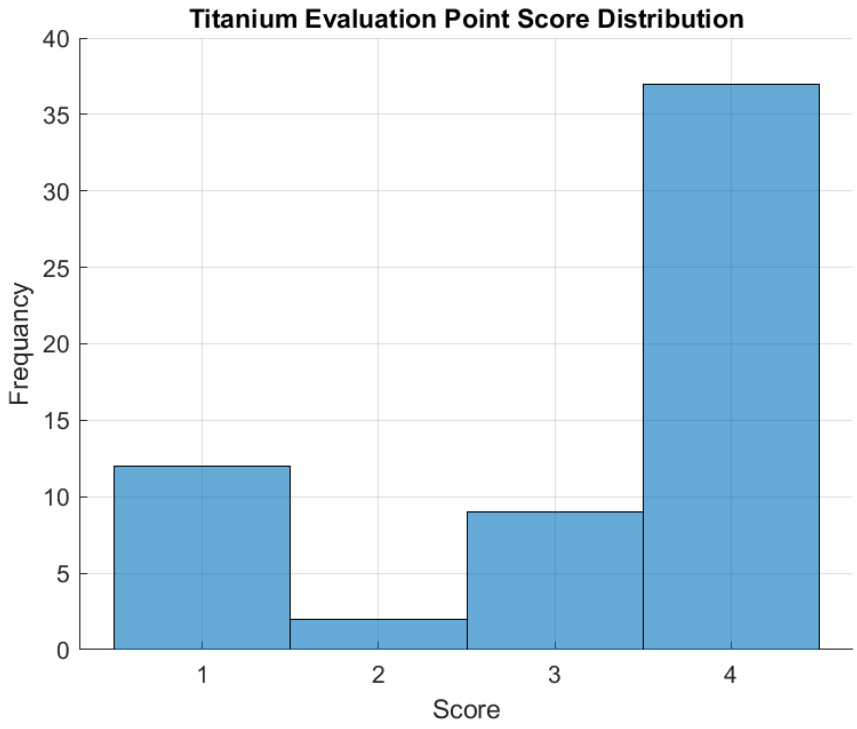

Figure 5.3: Distribution of Evaluation Scores, Titanium

The visual formability evaluation results also highlights the need to perform such a procedure as one of the titanium heats (C4) is significantly and consistently poorer performing than the other 4. Table 5.1 shows how similar all 5 heats are, and how there is no obvious indication of formability based on the material properties provided by the supplier.

Heat	Supplier	σ_Y(L/T) [MPa]	σ_T(L/T) [MPa]	EL(L/T) [%]	Heat Treatment
C1	C	184 / 212	324 / 321	47 / 34	Annealed
C2	C	176 / 212	325 / 313	46 / 34	Annealed
C3	C	199 / 209	328 / 317	46 / 34	Annealed
C4	C	199 / 209	328 / 317	46 / 34	Annealed
D1	D	201 / 246	326 / 318	48 / 36	Annealed & Pickled

Table 5.1: Material Properties Summary, L = Longitudinal, T = Transverse

5.2 Scanning

Due to time limitations, and time required to perform a scan of a single plate, only a limited number plates have been scanned. In order to maximise the data extracted from each scan, the evaluation of points on the titanium heats were expanded from the original 15 points to 60 points. In order to minimise the effect the point geometry has on the total evaluation score, the rotational symmetry of the test plates were used to pick 3 additional sets of 15 evaluation points. The additional 3 sets are referred to as set B, set C and set D, with set A being the original set of 15 points. It is important to note that although the point geometry is the same for each set, formability scores are expected to vary between each set due to the anisotropic nature of titanium. As such that additional sets are used only to study the relationship between the geometric properties of the plates and the visual scores at the evaluation point. The plots for minimum thickness and maximum thickness gradient against visual score are plotted again with the additional evaluation points in Figure 5.4 and 5.5 respectively.

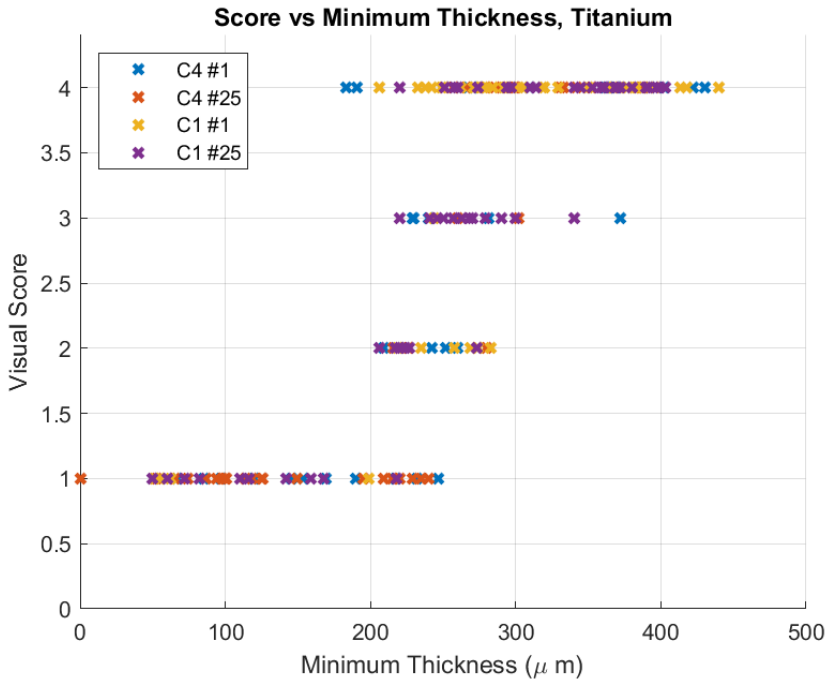

Figure 5.4: Visual score and Minimum thickness at additional evaluation points, Titanium

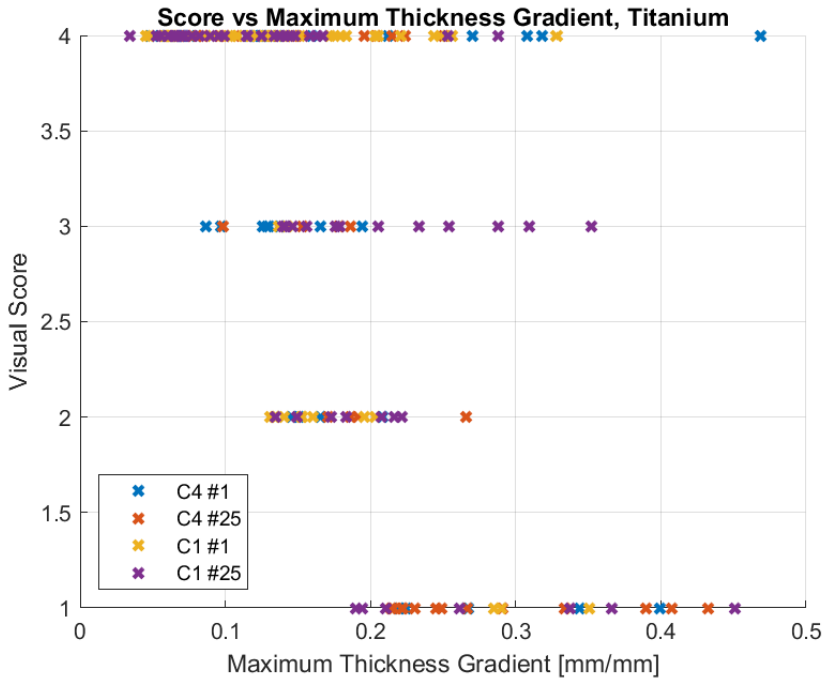

Figure 5.5: Visual score and Maximum Thickness Gradient at additional evaluation points, Titanium

5.2.1 Scanning Results Limitations

Initial investigation of the data obtained from 3D scan shows that important plate properties, such as material thickness can be captured by the equipment and procedure. To check the validity of the scans, the material volume of each scanned plate is calculated. Assuming there is no compressibility of the material during pressing, the volume of the plate before and after pressing should be the same. As the blank geometry is known, the blank volume is:

$$V_0 = 330 \times 330 \times 0.5 = 54,450\text{mm}^3 \tag{7}$$

The area and average sheet thickness is obtained from the scan data and the presses plate volumes are calculated and compared to V_0 in Table 5.2.

Plate	Area[mm^2]	Average thickness [mm]	Volume [mm^3]	Error [%]
A1 #1	126,555	0.447	56,570	3.894
A1 #25	125,632	0.439	55,152	1.290
A2 #1	126,457	0.446	56,400	3.581
A2 #5	126,879	0.430	54,558	0.199
C4 #1	122,206	0.448	54,748	0.548
C4 #25	122,906	0.446	54,816	0.672
C1 #1	122,240	0.446	54,519	0.127
C1 #25	123,759	0.446	55,197	1.371

Table 5.2: Volume of Scanned Plates

The volume calculated from the scan differs less than 4% than the expected volume.

The scale of the minimum surface defect detectable by the scan results, can be found by approximating the spatial resolution of the scans. Each scan has approximately 140×10^6 scan points and a surface area approximately 2 times the area shown in Table 5.2 (both sides of the plate), the average being $249,158\text{mm}^2$. The resolution of the scans is approximately 560 px/mm^2 or about $40\mu\text{m}$.

For titanium pressings, a general trend between formability score at each evaluation point and minimum material thickness at the evaluation point was observed, however two issues were identified with the minimum material thickness data.

1. Cracks identified at some evaluation points during the visual inspection had minimum thickness greater than 0mm.

2. There exists an overlap between formability scores and minimum material thickness in the range $200\mu m \leq t \leq 300\mu m$ that makes it impossible to observe a one to one relationship.

5.3 Metrics for Formability

5.3.1 Thickness Profile - Defect Detection

Figure 4.6 highlights the issue of trying to detect small cracks using the scan data, as the evaluation points identified as having cracks (red lines) have a minimum thickness greater than zero. An example of such a point is presented in Figure 5.6, a crack was observed at this point, yet the minimum thickness is approximatly 130 μm

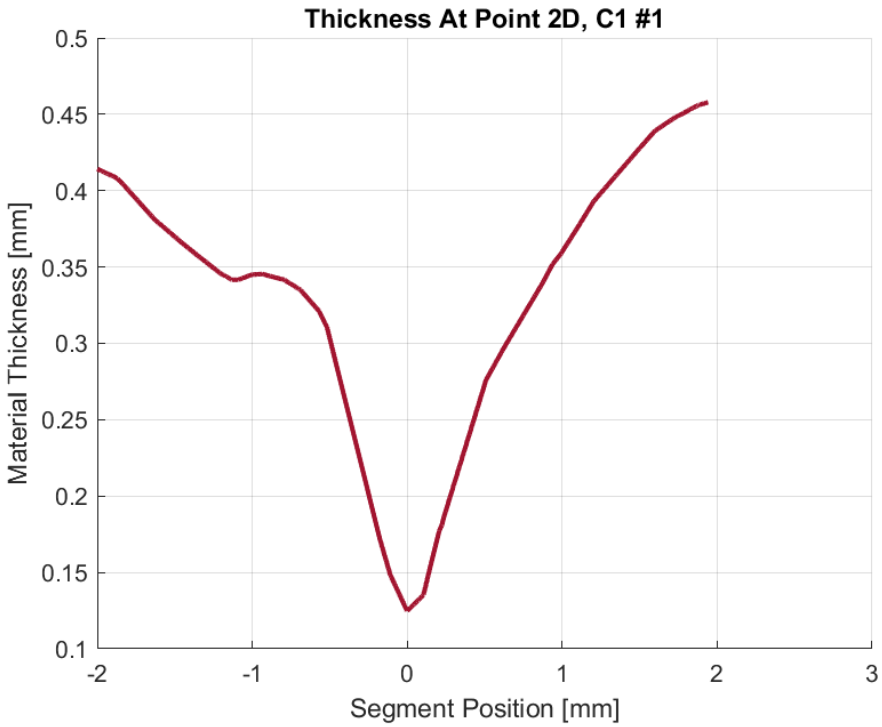

Figure 5.6: Crack Point Thickness Profile

Imagery and measurement of the crack in Figure 5.7 shows that the width of the crack is about 60 μm, which is approaching the resolution of the scan, and explains why it is difficult to detect cracks of this size in the thickness profile.

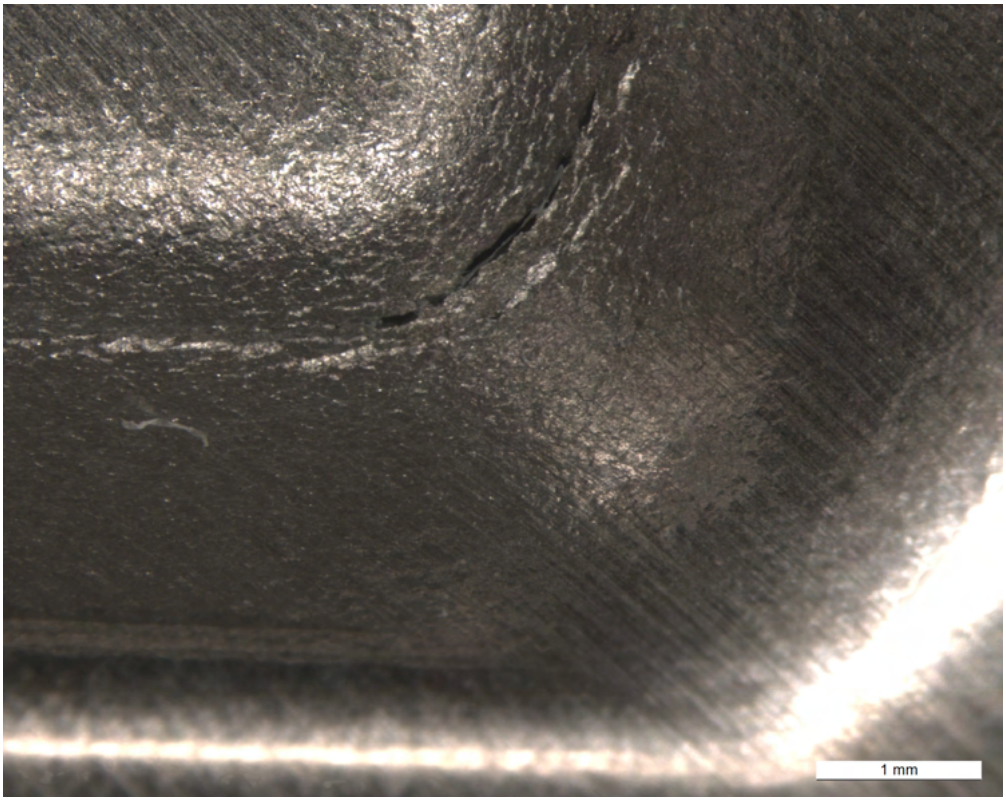

Figure 5.7: Crack Point Imagery (20x)

Cracks are expected to occur within regions of local necking, and the width of the local necking is expected to be similar to the material thickness, ($t = 500\mu$m). So necking near cracks and the onset of necking should be detectable in the thickness profile. Plotting select thickness profile curves of cracked points with vertical lines at ± 0.25mm from the minimum thickness illustrates the expected necking region, for crack points and necking points Figure 5.8 (a) and (b) respectively.

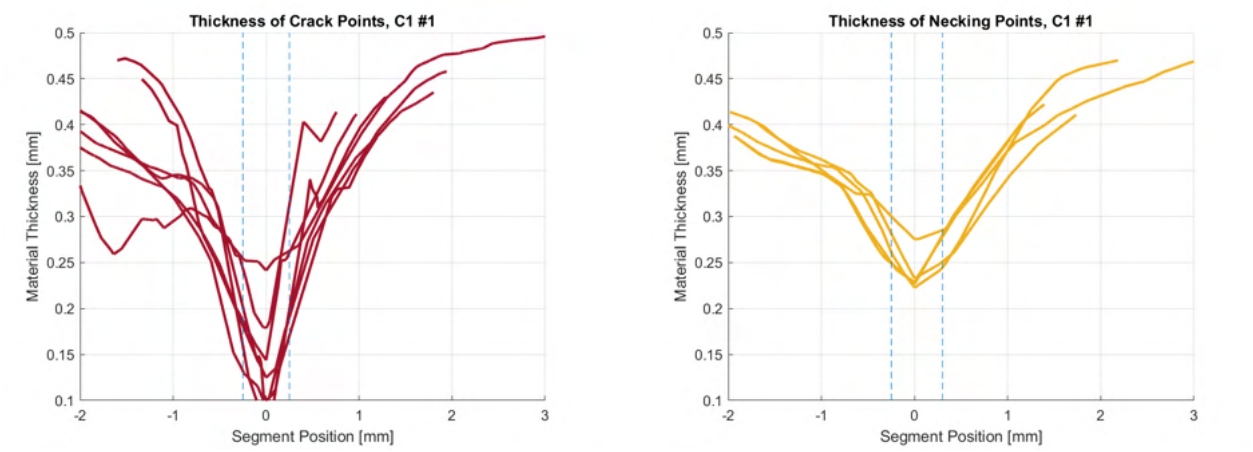

(a) Crack Point Profiles

(b) Necking Point Profiles

Figure 5.8: Surface Defect Point Profiles, With Expected Necking Zone

Large cracks, on the other hand are easily identified in the scanning data as there is a discontinuity in the thickness profile. For example, there is a large crack at point 3C on plate C1 #1, see Figure 5.9.

Figure 5.9: Large Crack

The width of the crack at its widest is about 1.5mm, Figure 5.10 shows the scan location and the thickness profile, with a discontinuity between 0 and 1.25mm.

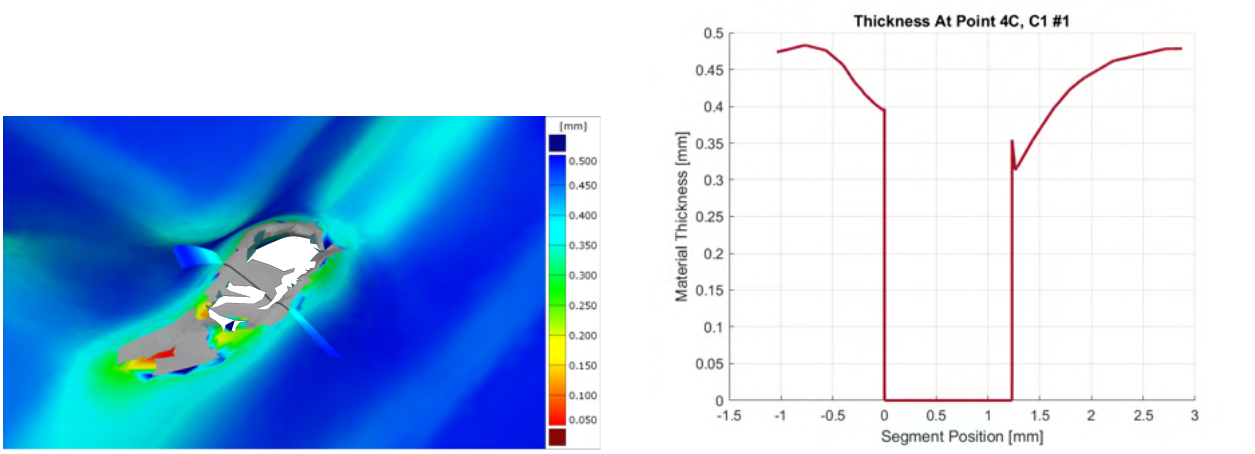

(a) Large Crack at Evaluation Point

(b) Thickness Profile at Large Crack

Figure 5.10: Large Crack in Scan Data

5.3.2 Minimum Thickness

Although small cracks are represented in the scans with a thickness greater than 0mm, they generally have a smaller minimum thickness than the necking points, meaning that they can be estimated. To test that small cracks can be estimated, Figure 4.10 is replotted, this time omitting evaluation points with 0mm minimum thickness, see Figure 5.11.

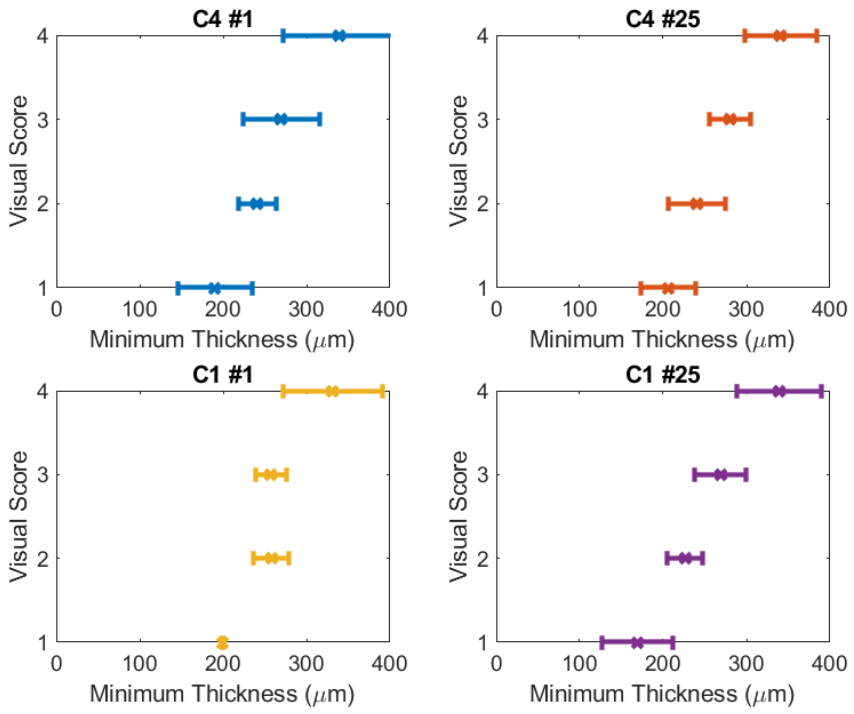

Figure 5.11: Minimum Thickness vs Visual Score with 0mm thickness omitted

As expected the average minimum thickness for score 1 increases when the points with 0mm minimum thickness are omitted, increasing from about 100-150 μm to 150-200 μm, however, there remains a distinction between score 1 and 2.

Figure 5.12 plots average thickness and standard deviation for each score for all 4 titanium plates with 0mm miniumum thickness points omitted. A linear line has been fitted to the data, which shows a strong correlation between the average minimum thickness and the visual score.

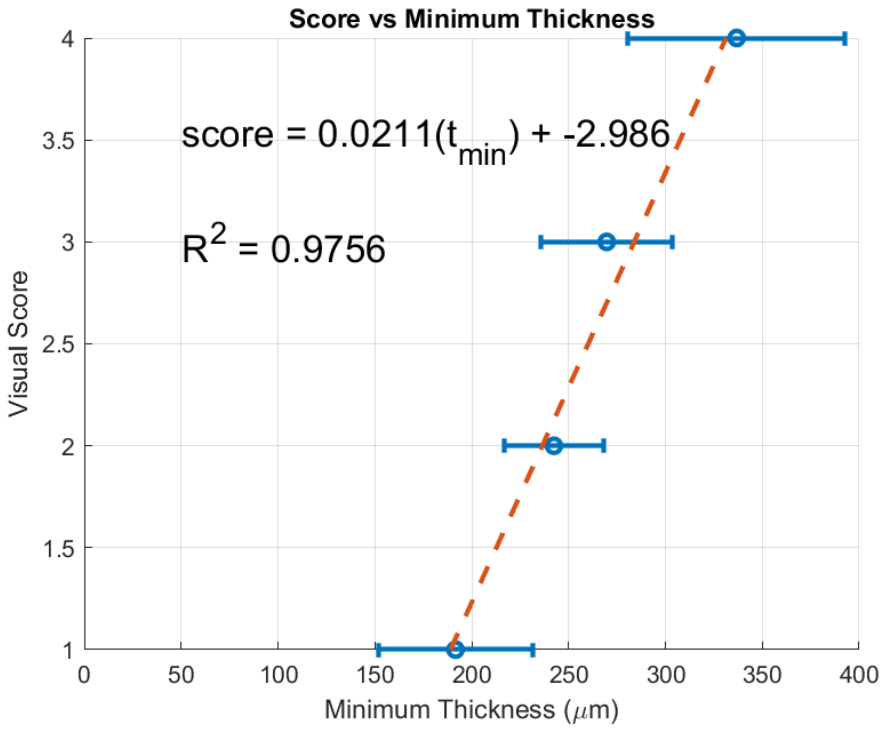

Figure 5.12: Minimum Thickness vs Visual Score with 0mm thickness omitted, all Ti plates

An evaluation score model, based on the minimum thickness at each point is proposed;

$$\text{score}(t_{min}) = \begin{cases} 0.0211(t_{min}) - 2.986 & \text{if } t_{min} \geq 0 \\ 0 & \text{if } t_{min} = 0 \end{cases} \tag{8}$$

This model is tested against the visual score results for the 4 titanium plates and presented in Table 5.3

Plate	Total Visual Score [%]	Model Score [%]	Error [%]
C4 #1	78	82	4.2
C4 #25	58	66	13.7
C1 #1	95	95	0.1
C1 #25	82	80	2.4

Table 5.3: Minimum Thickness Model vs Visual Score

The proposed model performs well when predicting the formability of plates with high formability scores, however performs poorly for lower formability.

5.3.3 Thickness Gradient

The points with 0mm miniumum thickness are also omitted for the computations for the average maxiumum thickness gradient for each score and is replotted in Figure 5.13.

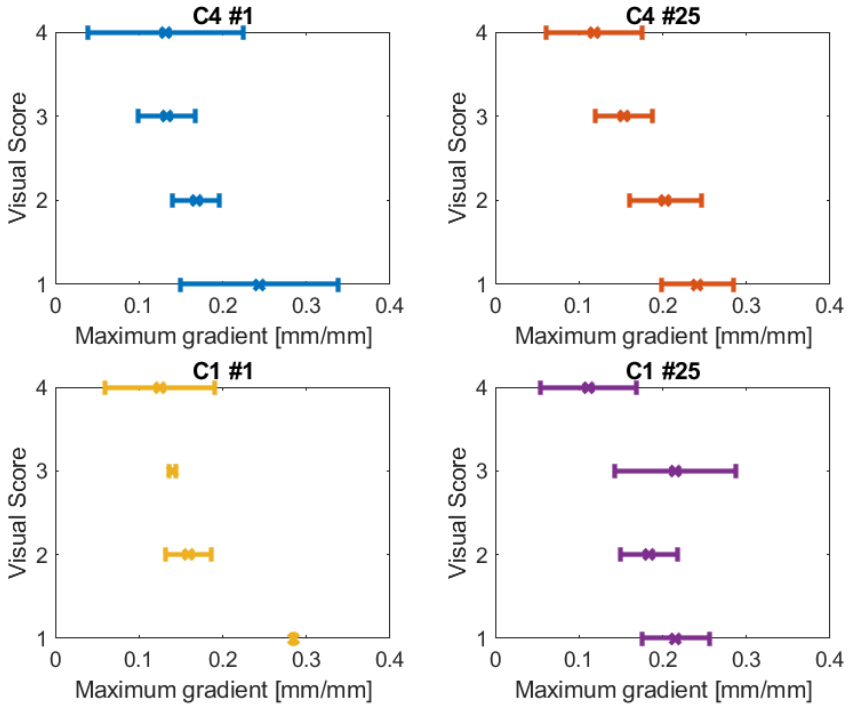

Figure 5.13: Maximum Gradient vs Visual Score with 0mm thickness omitted

The average and standard deviation of the maximum gradients for each score across all 4 titanium plates is plotted and a linear relation is plotted in Figure 5.14. Although there is a decreasing trend, there is significant overlap between the scores and there exists an overlap between all 4 scores for maximum gradients between approximately 0.15 and 0.2.

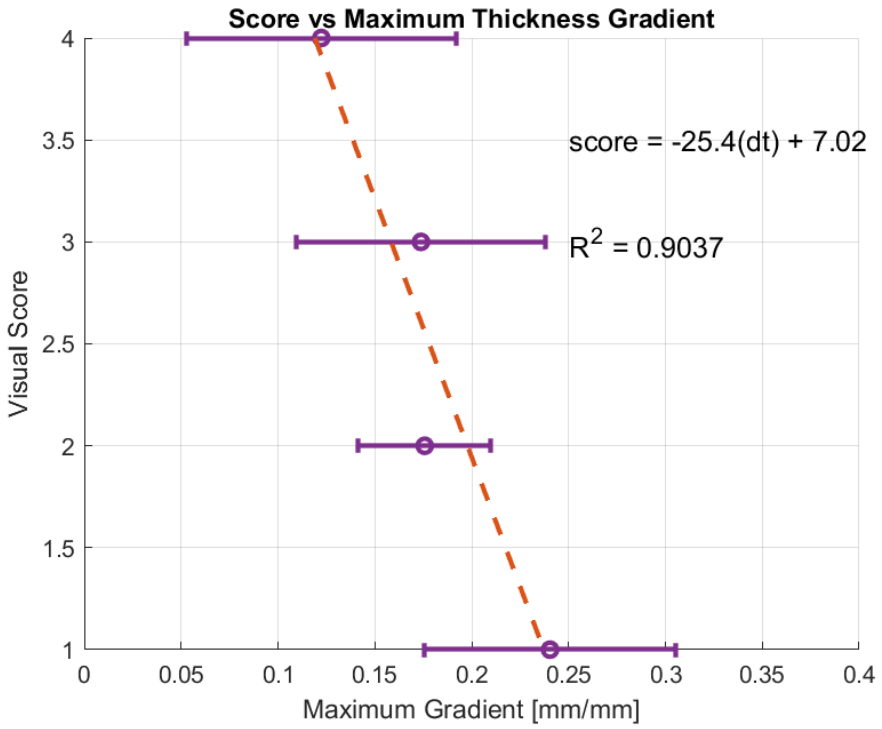

Figure 5.14: Maximum Gradient vs Visual Score with 0mm thickness omitted, all plates

An evaluation score model based on the maximum gradient at each point is proposed;

$$\text{score}(dt_{max}) = \begin{cases} -27.8(dt_{max}) + 7.41 & \text{if } t_{min} \geq 0 \\ 0 & \text{if } t_{min} = 0 \end{cases} \tag{9}$$

Plate	Total Visual Score [%]	Model 2 Score [%]	Error [%]
C4 #1	78	72	8.6
C4 #25	58	59	1.7
C1 #1	95	88	7.7
C1 #25	82	70	14.8

Table 5.4: Minimum Thickness Model vs Visual Score

The model based on the maximum thickness gradient performs poorly, with no apparent trend between error and formability.

5.4 Effects of Strain State

3 patterns of strain states were identified that relate closely to the geometry at the evaluation point. The 3 types of points that were identified were;

- Corner Point (points 1,2,5,8,11,13,14,15)

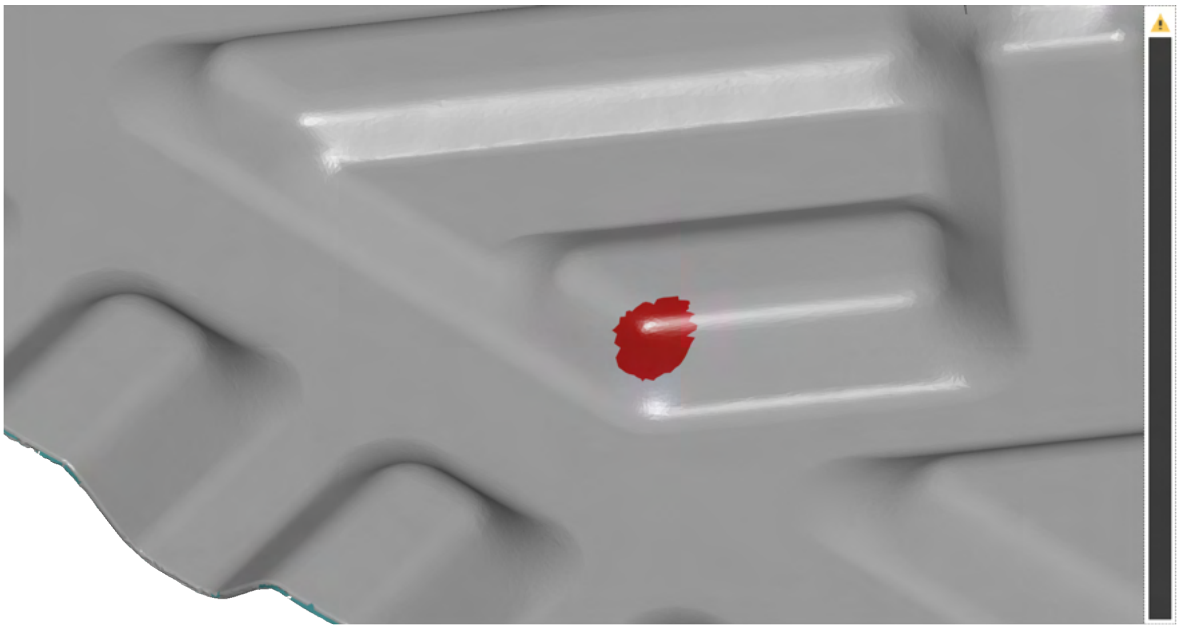

Figure 5.15: Corner Bend Point Example (point 8)

- Edge Point (6,7,9,12)

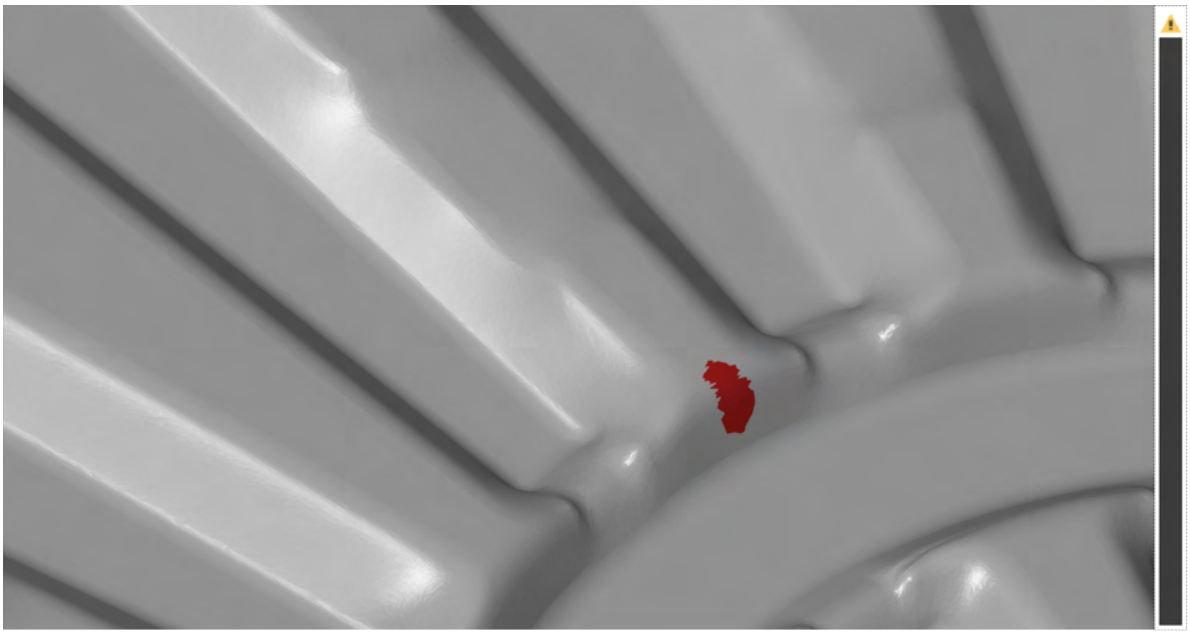

Figure 5.16: Edge Bend Point Example (point 6)

- small radius bends (3,4,10)

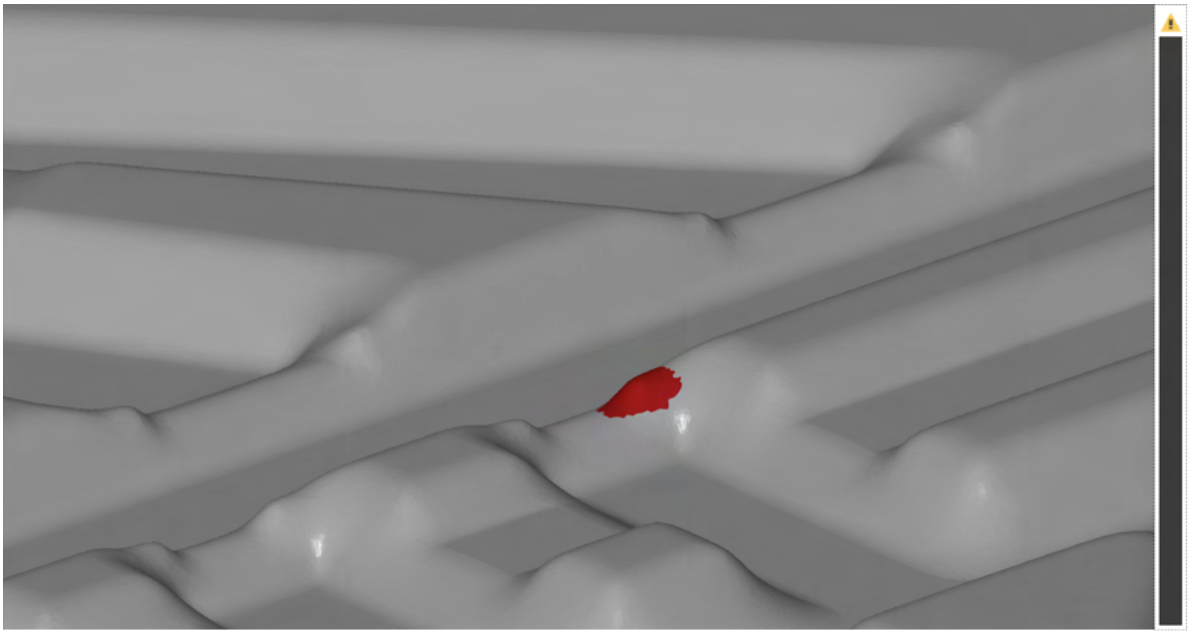

Figure 5.17: Small Radius Point Example (point 4)

These geometries have an effect on the strain state which is reflected in the simulation data.

Analysis of 316L and titanium produced similar results, the FLD for each point type for titanium are presented in Figures 5.18, 5.19 and 5.20

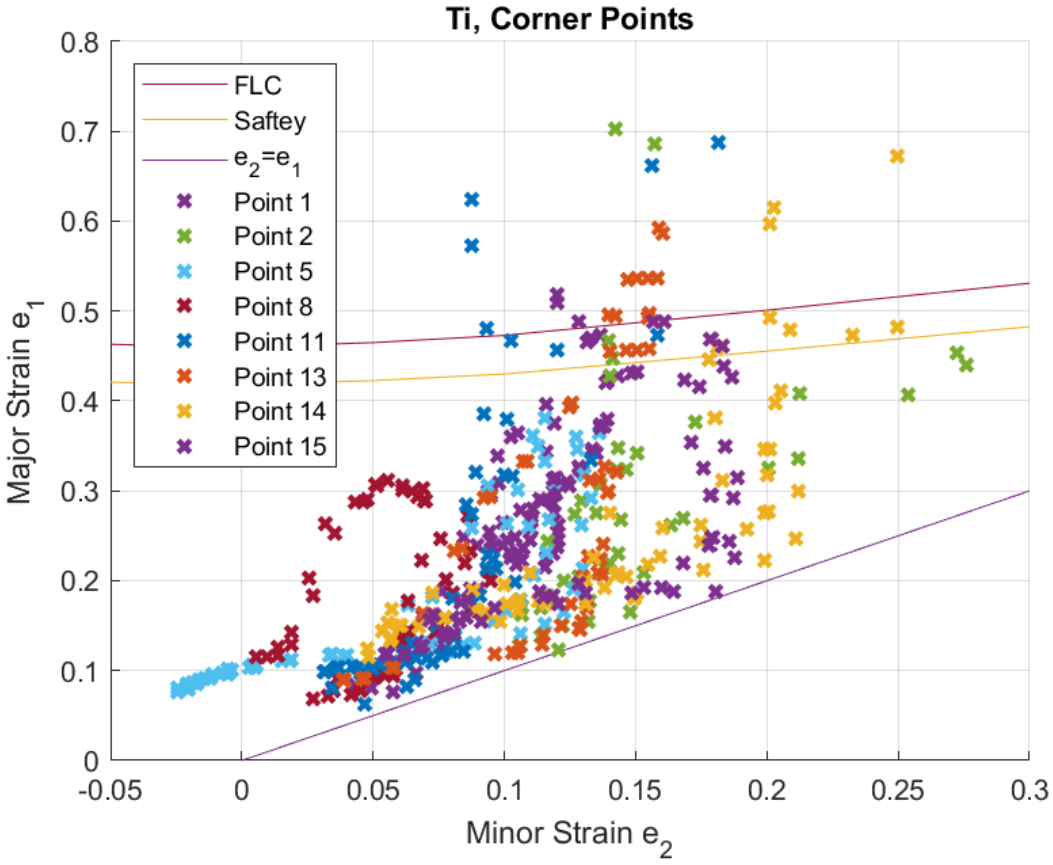

Figure 5.18: Corner Points FLD

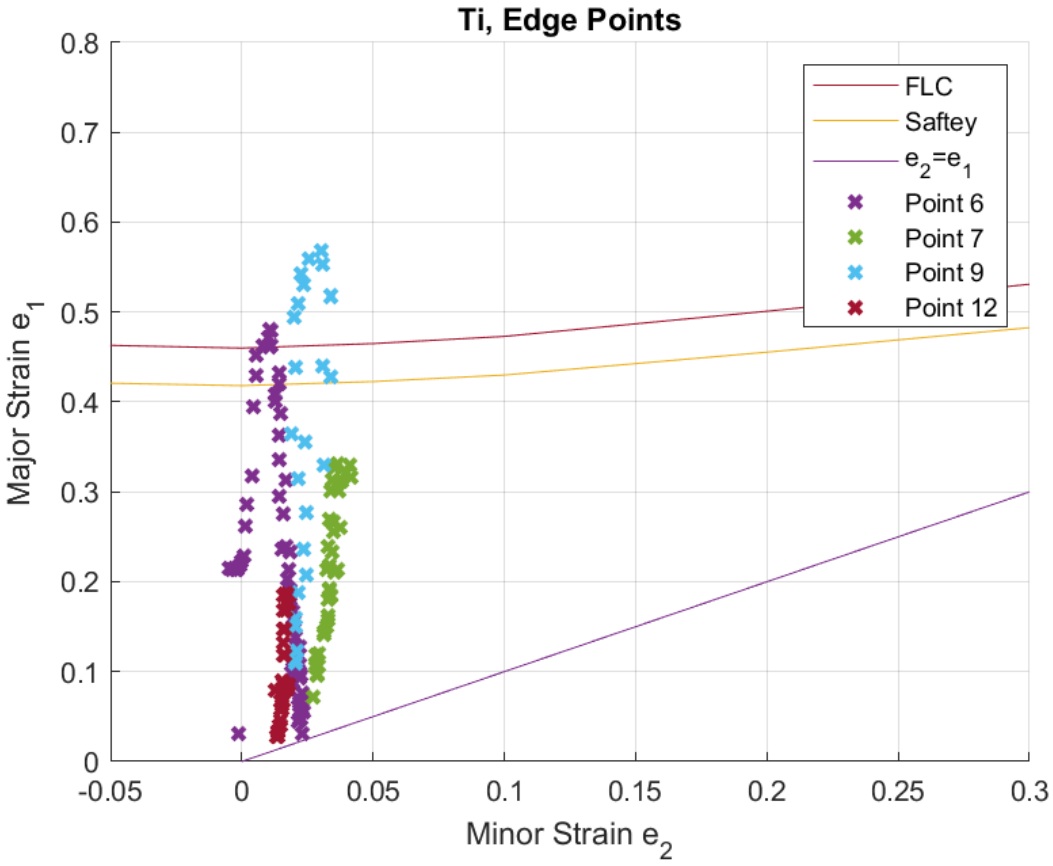

Figure 5.19: Edge Points FLD

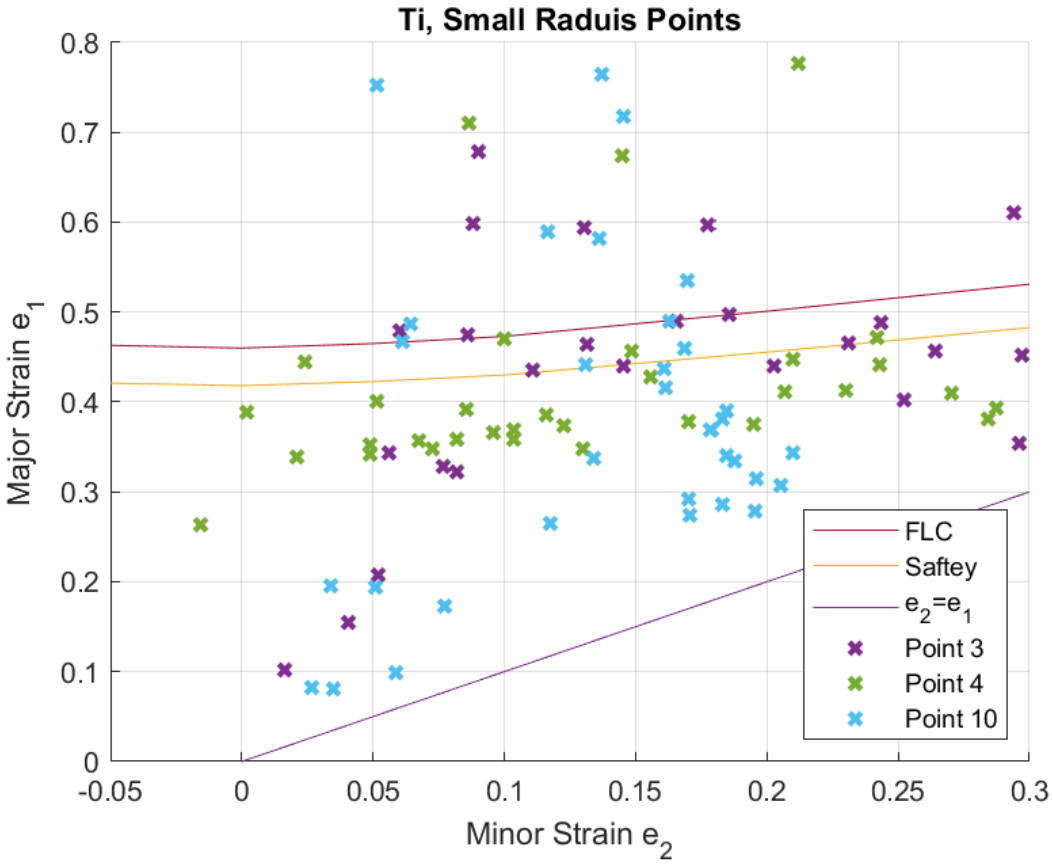

Figure 5.20: Small Radius Points FLD

5.4.1 Strain Ratios

The analysis of the strain states at the 15 evaluation points using the forming simulation highlighted the potential difficulty in using the scan data alone to predict formability, as the different geometries of the evaluation points result in very different strain states.

FEM IS ACCURATE, COMMENT ON METHOD USED TO FIND B

From the forming limit curves for each evaluation point the maximum principal strains (ϵ_1 and ϵ_2) and ratios (β) are shown in Table 5.5. The table is ordered by β and grouped by geometry type.

Point	ϵ_1	ϵ_2	β
6	0.480	0.011	0.02
9	0.568	0.030	0.05
12	0.186	0.016	0.09
7	0.331	0.037	0.11
2	0.685	0.157	0.23
1	0.509	0.120	0.24
11	0.661	0.156	0.24
13	0.592	0.159	0.27
5	0.382	0.116	0.30
8	0.272	0.086	0.31
15	0.488	0.161	0.31
14	0.492	0.181	0.37
10	0.342	0.210	0.61
3	0.451	0.297	0.66
4	0.393	0.287	0.73

Table 5.5: Evaluation Point Approximate Strain Ratios, Titanium

From Table 5.5 it can be seen that different point geometries have different strain ratios;

- Edge Points, $\beta < 0.15$
- Corner Points, $0.2 < \beta < 0.4$
- Small Radius Points, $\beta > 0.6$

5.4.2 Effects of Strain Ratios

The minimum thickness and maximum gradient for the identified types of points have been analysed separately. Figure 5.21 plots the miniumum thickness by point type.

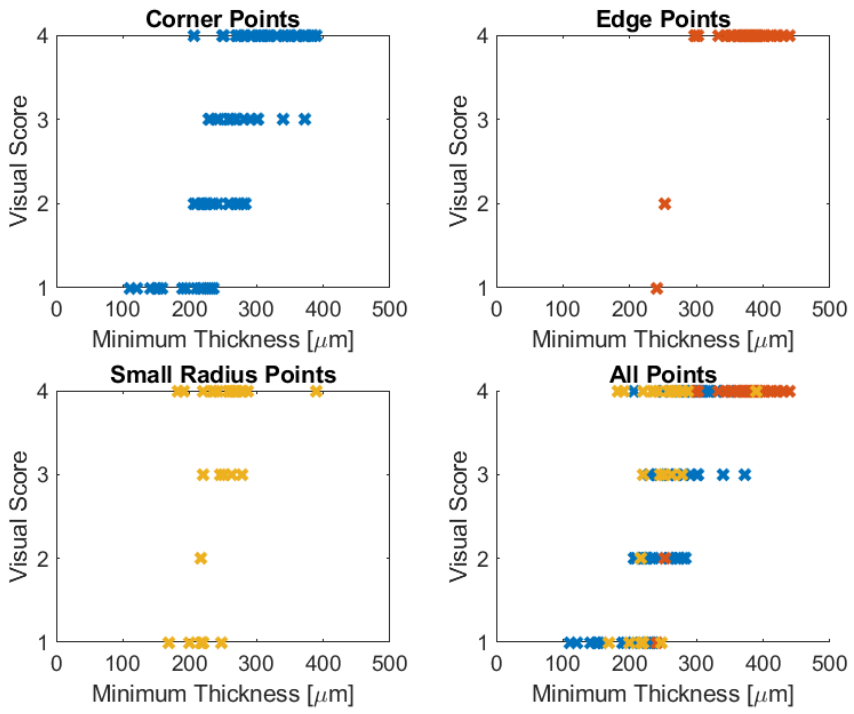

Figure 5.21: Minimum Thickness Plotted by Bend Type

As the small radius points have β ratio closer to 1 (i.e closer to biaxial stretching condition) than the other types of points it is expected that these points can undergo more thinning before surface defects develop. This is observed in the above figure as a number of small radius points with a score of 4 have a minimum thickness less than 200 μm. As the correlation between the minimum thickness and the visual score for small radius points is weaker than other point geometries, there effect on the miniumum thickness based model is tested by omitting the small radius points from the analysis. Figure 5.24 presents the average minimum thickness and standard deviation for each score, only for corner and edge points.

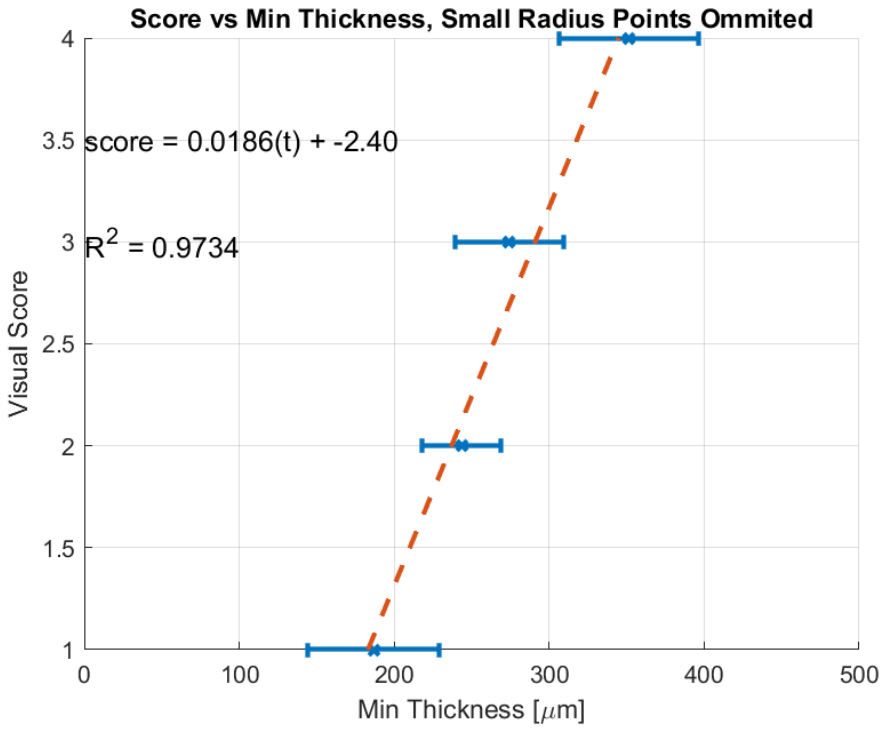

Figure 5.22: Thickness Average and std. by score

Comparing Figures 5.12 and 5.24 it is seen that the evaluation point geometry has a minimal effect on the relationship between the minimum thickness and visual score. However, the effect on the maximum thickness gradient appears to be stronger as seen in Figure 5.23.

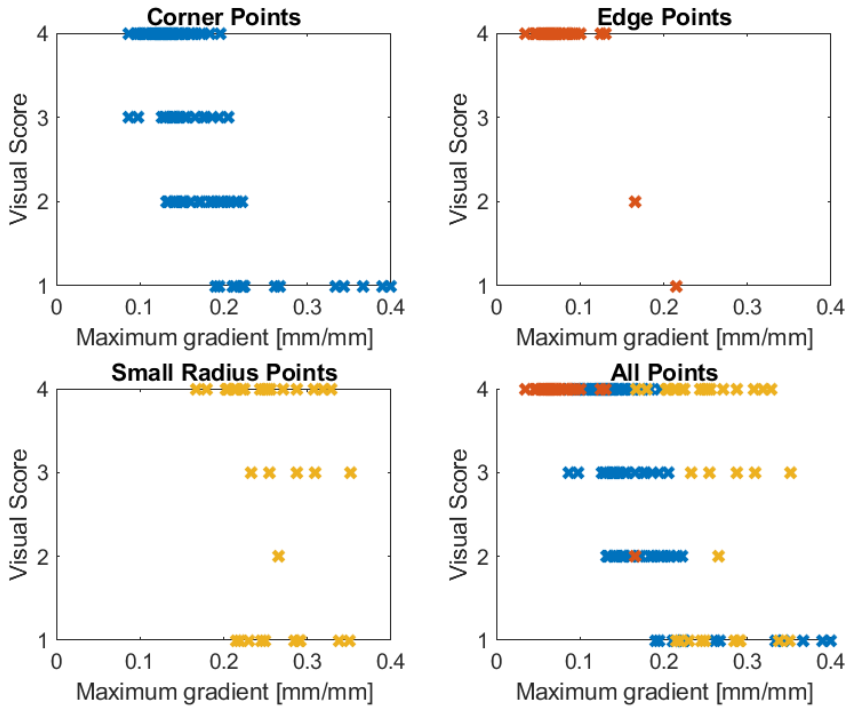

Figure 5.23: Thickness Gradient Plotted by Bend Type

It is clear from Figure 5.23 that the relationship between point visual score and maximum gradient is stronger for corner points and edge points compared to small radius points. The analysis performed in the previous section is repeated, this time omitting the small radius points, see Figure 5.24

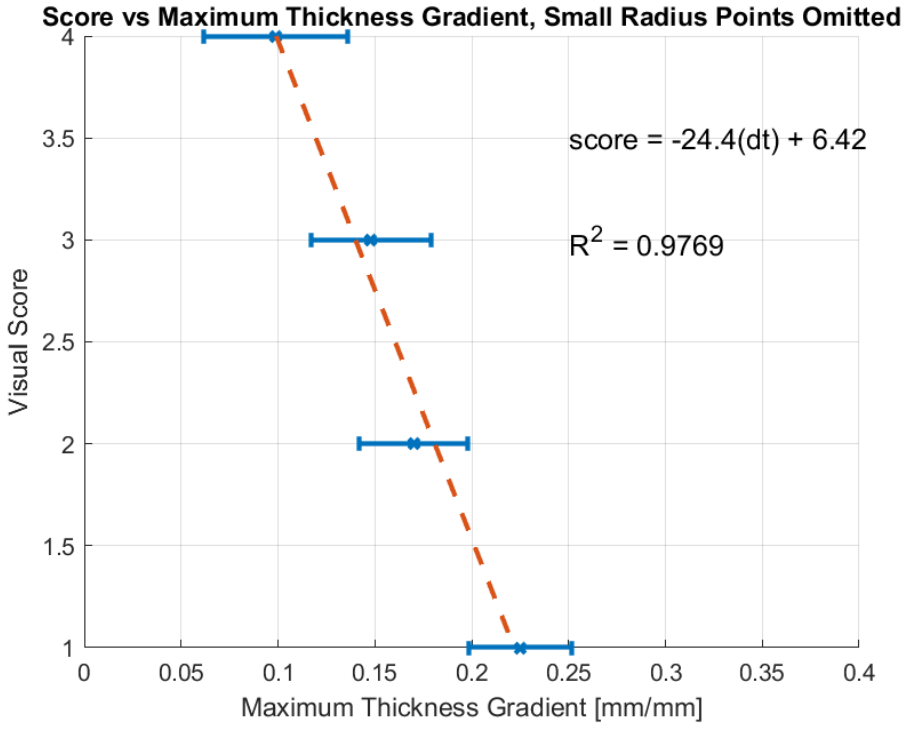

Figure 5.24: Thickness Gradient Average and std. by score

By omitting the small radius points from the gradient analysis, the spread of gradients for each score is reduced and a stronger correlation is observed. The formability model based on the maximum thickness gradient is modified to only include corner (P_C) and edge (P_E) points.

$$\text{score}\mathrm{P_C}, \mathrm{P_E}(dt_{max}) = \begin{cases} -24.4(dt_{max}) + 6.42 & \text{if } t_{min} \geq 0 \\ 0 & \text{if } t_{min} = 0 \end{cases} \tag{10}$$

Testing this modified model does indeed show a reduction in the overall error in the predicted formability score compared to the unmodified maximum gradient based model, see Table 5.6.

Plate	Total Visual Score [%]	Model 2b Score [%]	Error [%]
C4 #1	78	78	0.12
C4 #25	58	61	5.4
C1 #1	95	89	5.5
C1 #25	82	74	9.5

Table 5.6: Maximum Gradient (Corner and Edge Points) Model vs Visual Score

The weak relation between the visual score and the maximum thickness gradient for the small radius points is difficult to explain. A possible explanation for this is due to the greater minor strains (ϵ_2) at these points, which has a stabilizing effect on necking development, as described by Marciniak et. al.

Table 5.7 summarise the performance of the 3 proposed models.

Plate	Error 1 [%]	Error 2a [%]	Error 2b [%]
C4 #1	4.2	8.6	0.12
C4 #25	13.7	1.7	5.4
C1 #1	0.1	7.7	5.5
C1 #25	2.4	14.8	9.5

Table 5.7: Model Performance

As only a limited number of titanium plates were scanned, it is difficult to draw conclusions about the relative performance of the models.

5.5 Comparison Between Titanium Heats and 316L Heats

5.5.1 Thickness Profile

The increased formability of 316L over titanium is well represented by the difference in the thickness profiles at the evaluation points, see Figure 5.25. In the visual score for the 316L heat all points are 4 (no defect), while for the titanium heat, points 1 and 5 are 4 (no defect), in contrast with points 2 and 14 which are 1 (small crack).

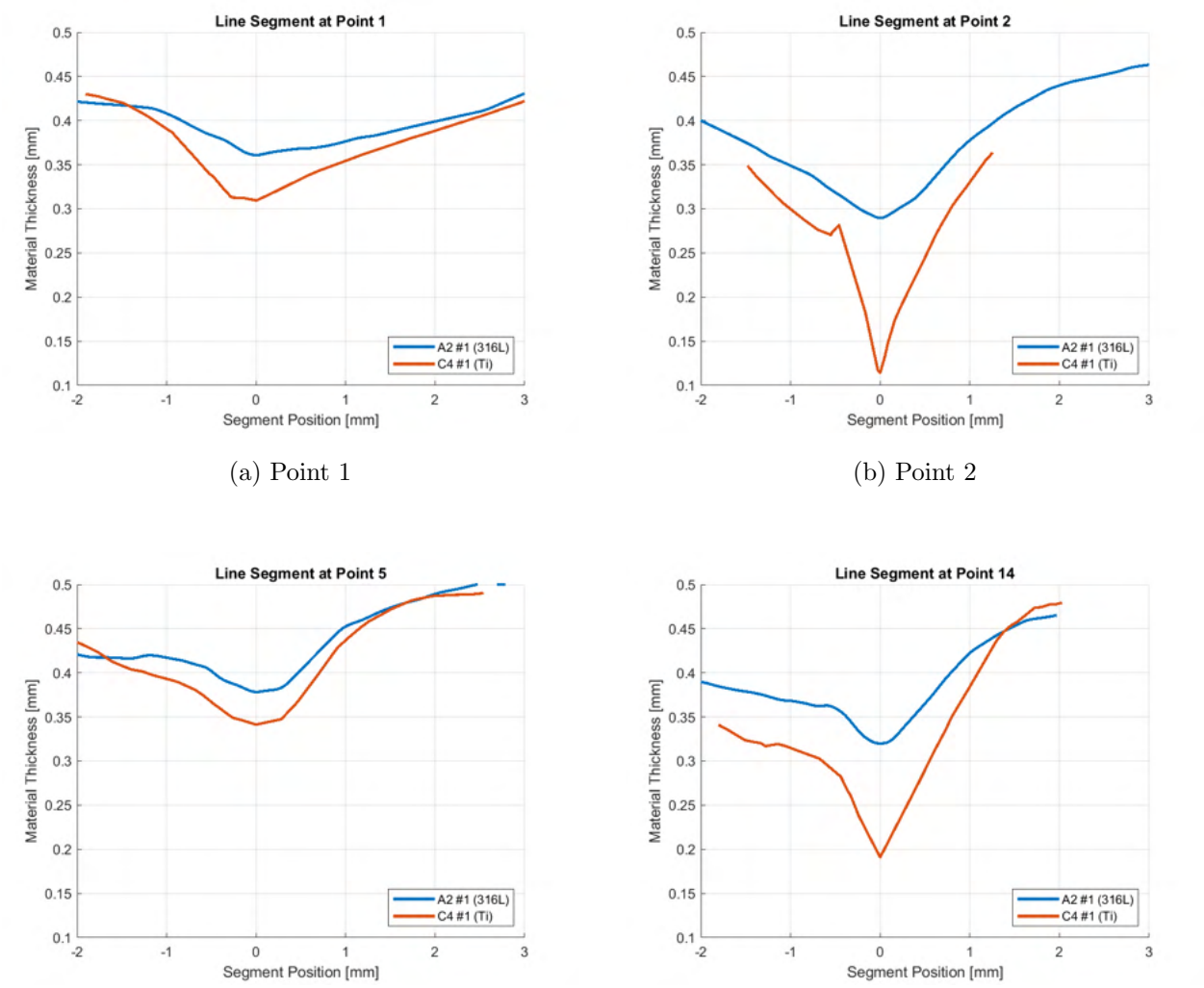

(a) Point 1

(b) Point 2

(c) Point 5

(d) Point 14

Figure 5.25: Thickness Profile Comparison

5.5.2 Formability and Press Number Relationship

The results from the scan data were used to investigate the observed behaviour concerning the relationship between formability and press number. The observed relationship between formability and press number for 316L and Titanium was in agreeance with previous observations, that is; there is little to no relationship between formability and press number for 316L while there is a negative relationship between formability and press number for titanium (Figure 4.1).

Therefore the material thickness profile is expected to remain unchanged between press #1 and press #25 for 316L, while a change in the profile, resulting in a smaller minimum thickness and a greater maximum thickness gradient is expected for titanium plates. This behaviour is well captured at point 5, Figure 5.26.

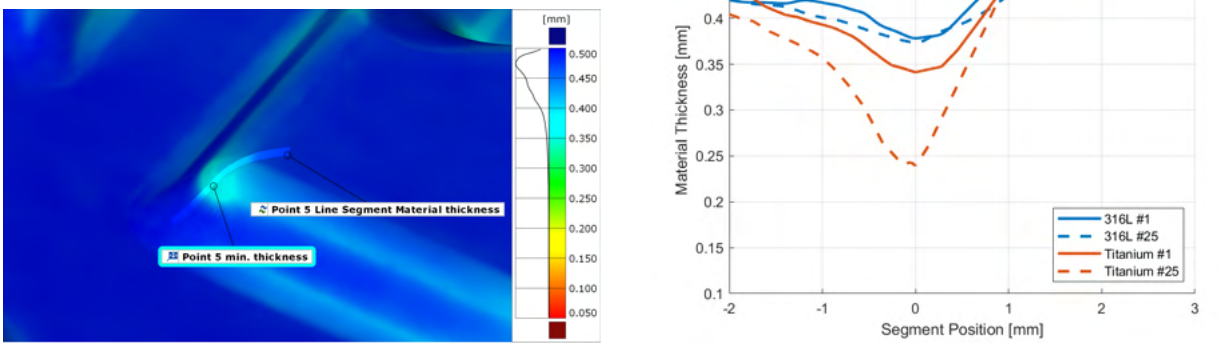

(a) Point 5 Evaluation Point

(b) Point 5 Thickness Profile

Figure 5.26: Comparison of Thickness Profiles between 316L and Ti and press number

The change in formability is believed to be a result of the accumulation of adhered material to the tool when pressing titanium due to galling. This project has not confirmed the presents of galling on the tool as it is outside the scope of this project. However, previous investigations at Alfa Laval have detected the presents of galling using SEM imaging.

5.6 Discussion Summary

This chapter investigated the following topics

- The issues with the current visual formability evaluation
- The limitations of the 3D scanning results in relation to detecting small cracks
- Ways of predicting small cracks when the minimum thickness is greater than 0mm
- The formulation and testing of a linear relation between the minimum thickness and the visual score for individual evaluation points for titanium plates
- The formulation and testing of a linear relation between the maximum thickness gradient and the visual score for individual evaluation points for titanium plates
- The effects of evaluation point geometry and strain state on the two identified metrics
- The effects of evaluation point geometry and strain state on the proposed models
- A comparison between the thickness profile for 316L and titanium and the effect of press number on the thickness profile

6 Conclusion

This project set out to answer the question, Can material thickness measurements be used to evaluate sheet metal material formability and replace the current visual formality evaluation? In relation to objectives, the following findings have been presented;

1. **To verify that 3D scanning can be used to measure material thickness and other typical pressing defects**
    - 3D Scanning was shown to be able to capture the thickness of the pressed plates.
    - Surface defects that are smaller than about 0.1mm are difficult to measure using 3D scanning due to scanning resolution limits.
    - Although not directly detectable, extreme material thinning at evaluation points was used as evidence of existence of small cracks
    - Material necking was detected by the material thickness data
2. **To identify relationship between material thickness and surface defects**
    - Due to the limited range of formability of the investigated 316L heats, it is was not possible to develop strong relationships between material thickness and surface defects.
    - Due to the wider range of surface defects present on the investigated titanium heats, a relation between the material thickness and surface defects was observed for this material
    - Thickness profile, minimum thickness and maximum thickness gradient were identified as metrics for identifying surface defect
3. **To evaluate material formability based on the material thickness and compare predictions to results from the current formability evaluation**
    - The strength of the identified metrics were evaluated by comparing them to the visual formability score.

- The minimum thickness metric performed better than the maximum thickness gradient metric when compared to the total visual evaluation score.
- There was a stronger linear correlation between the minimum thickness and evaluation point score ($R^2 = 0.98$) than the maximum thickness gradient and evaluation point score ($R^2 = 0.90$).

4. **To provide physical explanations of the identified relationships**

   - Forming simulation results were used to investigate strain states at evaluation points and provided physical explanations into observed relationship.
   - Evaluation point geometry was shown to strongly influence the strain state at the evaluation points.
   - Variations in the relationship between material thickness and surface defects were shown to be influenced by the strain state at the evaluation points

Definitive answer of the research question is not possible due to the following project limitations;

- The limited number of scans makes it difficult to draw conclusions about the accuracy of the proposed formality models based on material thickness
- Further analysis on 316L heats were not possible due to the limited range of surface defects detected in the material

6.1 Future Work

3D scanning shows a promising potential to form the basis of an objective formability evaluation method. However, in order to develop and test formability models based on thickness data to replace the current evaluation method, more statistical analysis is required, which requires more scanning and evaluation data to be collected. In addition to collecting more data, the current understanding could be expanded beyond this projects narrow focus by investigating different:

- tool geometries
- lubricants
- materials and heat treatments
- blank thickness

One of the challenges with 3D scanning identified in this project is that the set up and measurement time required to perform the scanning is significantly greater than the time to complete the current visual inspection. Future work could investigate the possibility of using other methods for material thickness measurements. Future investigation of the relationship between formability and other, easier to measure dimensions like stretch and draw ratios, may yield usable metrics for predicting material formability.

References

[1] J. Hu, Z. Marciniak, and J. Duncan. *Mechanics of Sheet Metal Forming*. Elsevier Science, 2002.

[2] Ankita Awasthi, Kuldeep K. Saxena, and Vanya Arun. Sustainable and smart metal forming manufacturing process. *Materials Today: Proceedings*, 44:2069–2079, 2021. International Conference on Materials, Processing and Characterization.

[3] Stamping-forging processing of sheet metal parts — intechopen. (Accessed on 05/15/2023).

[4] R Pearce. *Sheet Metal Forming*. Adam Hilger, 1991.

[5] K. S. Sivakumaran. Role of yield-to-tensile strength ratio in the design of steel structures. 2010.

[6] Hiyam Farhat. *Operation, Maintenance, and Repair of Land-Based Gas Turbines*. Elsevier, 2021.

[7] https://upload.wikimedia.org/wikipedia/commons/c/c1/stress_strain_ductile.svg. `https://upload.wikimedia.org/wikipedia/commons/c/c1/Stress_strain_ductile.svg`. (Accessed on 05/25/2023).

[8] Surajit Paul, Manikandan Ganapathy, and Rahul Verma. Prediction of entire forming limit diagram from simple tensile material properties. *The Journal of Strain Analysis for Engineering Design*, 48:386–394, 08 2013.

[9] R. Hill. On discontinuous plastic states, with special reference to localized necking in thin sheets. *Journal of the Mechanics and Physics of Solids*, 1(1):19–30, 1952.

[10] H.W. Swift. Plastic instability under plane stress. *Journal of the Mechanics and Physics of Solids*, 1(1):1–18, 1952.

[11] Zdzislaw Marciniak and Kazimierz Kuczyński. Limit strains in the processes of stretch-forming sheet metal. *International Journal of Mechanical Sciences*, 9(9):609–620, 1967.

[12] Jianshe Lian and Dajun Zhou. Diffuse necking and localized necking under plane stress. *Materials Science and Engineering: A*, 111:1–7, 1989.

[13] S. Keeler and W. Backofen. Plastic instability and fracture in sheets stretched over rigid punches. *ASM Transactions Quarterly*, 56:25–48, 1961.

[14] Gorton M. Goodwin. Application of strain analysis to sheet metal forming problems in the press shop. *SAE Transactions*, 77:380–387, 1968.

[15] K Nakajima, T Kikuma, and K Hasuka. Study on the formability of steel 659 sheets, 1968.

[16] Scheme of the nakajima test according to en iso 12004-2. `https://www.researchgate.net/figure/Scheme-of-the-Nakajima-test-according-to-EN-ISO-12004-2_fig1_291141018`. (Accessed on 05/15/2023).

[17] Obtained flc points for different specimen widths. — download scientific diagram. `https://www.researchgate.net/figure/Obtained-FLC-points-for-different-specimen-widths_fig2_317260471`. (Accessed on 05/15/2023).

[18] Kenneth Cheong. *On the Influence of the Through-Thickness Strain Gradients for Characterization of Formability and Fracture of Sheet Metal Alloys*. PhD thesis, 01 2019.

[19] K. Isik, M.B. Silva, A.E. Tekkaya, and P.A.F. Martins. Formability limits by fracture in sheet metal forming. *Journal of Materials Processing Technology*, 214(8):1557–1565, 2014.

[20] Sante Dicecco, Clifford Butcher, M Worswick, E Boettcher, Edmund Chu, and C Shi. Determination of forming limit diagrams of aa6013-t6 aluminum alloy sheet using a time

and position dependent localized necking criterion. *IOP Conference Series: Materials Science and Engineering*, 159:012009, 11 2016.

[21] Leslie M. Bernick, Robert R. Hilsen, and Carl L. Wandrei. Development of a quantitative sheet galling test. *Wear*, 48(2):323–346, 1978.

[22] Erik Schedin. Galling mechanisms in sheet forming operations. *Wear*, 179(1):123–128, 1994.

[23] E. Schedin and B. Lehtinen. Galling mechanisms in lubricated systems: A study of sheet metal forming. *Wear*, 170(1):119–130, 1993.

[24] Houichi Kitano, Kuniaki Dohda, Mitjan Kalin, and Kornel F. Ehmann. Galling growth analysis in metal forming. *Manufacturing Letters*, 16:32–35, 2018.

[25] Dorel Banabic. *Sheet Metal Forming Processes, Constitutive Modelling and Numerical Simulation*. Springer Berlin, Heidelberg, 2010.